Inorg. Chem. **2006**, *45*, 1978–1996

Syntheses of $[F_5TeNH_3][AsF_6]$, $[F_5TeN(H)Xe][AsF_6]$, and F_5TeNF_2 and Characterization by Multi-NMR and Raman Spectroscopy and by Electronic Structure Calculations: The X-ray Crystal Structures of α- and β-F_5TeNH_2, $[F_5TeNH_3][AsF_6]$, and $[F_5TeN(H)Xe][AsF_6]$

Barbara Fir,[†] J. Marc Whalen,[†] Hélène P. A. Mercier,[†] David A. Dixon,[‡] and Gary J. Schrobilgen*,[†]

Department of Chemistry, McMaster University, Hamilton, Ontario L8S 4M1, Canada, and Department of Chemistry, University of Alabama, Tuscaloosa, Alabama 35487-0336

Received August 25, 2005

The salt, $[F_5TeN(H)Xe][AsF_6]$, has been synthesized in the natural abundance and 99.5% ^{15}N-enriched forms. The $F_5TeN(H)Xe^+$ cation has been obtained as the product of the reactions of $[F_5TeNH_3][AsF_6]$ with XeF_2 (HF and BrF_5 solvents) and F_5TeNH_2 with $[XeF][AsF_6]$ (HF solvent) and characterized in solution by ^{129}Xe, ^{19}F, ^{125}Te, ^{1}H, and ^{15}N NMR spectroscopy at –60 to –30 °C. The orange $[F_5TeN(H)Xe][AsF_6]$ and colorless $[F_5TeNH_3][AsF_6]$ salts were crystallized as a mixture from HF solvent at –35 °C and were characterized by Raman spectroscopy at –165 °C and by X-ray crystallography. The crystal structure of the low-temperature phase, α-F_5TeNH_2, was obtained by crystallization from liquid SO_2 between –50 and –70 °C and is fully ordered. The high-temperature phase, β-F_5TeNH_2, was obtained by sublimation at room temperature and exhibits a 6-fold disorder. Decomposition of $[F_5TeN(H)Xe][AsF_6]$ in the solid state was rapid above –30 °C. The decomposition of $F_5TeN(H)Xe^+$ in HF and BrF_5 solution at –33 °C proceeded by fluorination at nitrogen to give F_5TeNF_2 and Xe gas. Electronic structure calculations at the Hartree–Fock and local density-functional theory levels were used to calculate the gas-phase geometries, charges, Mayer bond orders, and Mayer valencies of F_5TeNH_2, $F_5TeNH_3^+$, $F_5TeN(H)Xe^+$, $[F_5TeN(H)Xe][AsF_6]$, F_5TeNF_2, and F_5TeN^{2-} and to assign their experimental vibrational frequencies. The $F_5TeN(H)Xe^+$ and the ion pair, $[F_5TeN(H)Xe][AsF_6]$, systems were also calculated at the MP2 and gradient-corrected (B3LYP) levels.

Introduction

The first example of xenon bonded to nitrogen, $FXeN(SO_2F)_2$, was synthesized[1] and characterized in the solid state by X-ray crystallography[2] and in solution by ^{19}F,[1,2] ^{15}N, and ^{129}Xe NMR spectroscopy.[2] Other imidodisulfurylfluoride species containing Xe(II)−N bonds have since been characterized by multi-NMR and Raman spectroscopy, namely, $Xe[N(SO_2F)_2]_2$,[3,4] $F[XeN(SO_2F)_2]_2^+$,[3−5] $XeN(SO_2F)_2^+$,[5] and $Xe[N(SO_2CF_3)_2]_2$.[6] The $[XeN(SO_2F)_2][Sb_3F_{16}]$[5] salt has been characterized by single-crystal X-ray diffraction. In all cases, xenon is bonded to an sp^2-hybridized nitrogen, and the stabilities of these species have been attributed to the high electronegativities[1−6] of their imidodisulfuryl ligands.

The Lewis acidity of the XeF^+ cation, as seen from the propensity of XeF^+ to form fluorine bridges with its counterion in its salts,[7] has been utilized in this laboratory to form numerous Xe(II)−N bonded cations by the reaction of an oxidatively resistant electron pair donor with the Lewis acid cation XeF^+.[8] Reactions of $[XeF][AsF_6]$ with neutral nitrogen bases in HF or of XeF_2 with protonated bases in BrF_5, accompanied by HF elimination, have led to XeF^+ adduct cations having sp- and sp^2-hybridized nitrogen. These include hydrogen cyanide,[9,10] alkylnitriles,[9] pentafluorobenzenenitrile,[9] perfluoroalkylnitriles,[9,11] perfluoropyridines,[12]

* To whom correspondence should be addressed. E-mail: schrobil@mcmaster.ca.
† McMaster University.
‡ University of Alabama.

(1) LeBlond, R. D.; DesMarteau, D. D. *J. Chem. Soc., Chem. Commun.* **1974**, 555.
(2) Sawyer, J. F.; Schrobilgen, G. J.; Sutherland, S. J. *Inorg. Chem.* **1982**, *21*, 4064.
(3) DesMarteau, D. D.; LeBlond, R. D.; Hossain, S. F.; Nöthe, D. *J. Am. Chem. Soc.* **1981**, *103*, 7734.
(4) Schumacher, G. A.; Schrobilgen, G. J. *Inorg. Chem.* **1983**, *22*, 2178.
(5) Faggiani, R.; Kennepohl, D. K.; Lock, C. J. L.; Schrobilgen, G. J. *Inorg. Chem.* **1986**, *25*, 563.
(6) Foropoulos, Jr., J.; DesMarteau, D. D. *J. Am. Chem. Soc.* **1982**, *104*, 4260.
(7) Selig, H.; Holloway, J. H. In *Topics in Current Chemistry*; Bosche, F. L., Ed.; Springer-Verlag: New York, 1984; pp 33−90.
(8) Schrobilgen, G. J. In *Synthetic Fluorine Chemistry*; Olah, G. A., Chambers, R. D., Prakash, G. K. S., Eds.; John Wiley & Sons: New York, 1992; pp 1−30.

10.1021/ic051451t CCC: $33.50
Published on Web 02/07/2006

and *s*-trifluorotriazine.[11] With the exception of the *s*-trifluorotriazine adduct, *s*-$C_3F_3N_2N-XeF^+$,[11] all of the adduct cations decompose below room temperature. The krypton(II) adduct cations, $HC\equiv N-KrF^{+}$[13] and $R_FC\equiv N-KrF^+$ ($R_F = CF_3$, C_2F_5, *n*-C_3F_7),[11] are unstable above ca. −50 °C and have also been characterized in this laboratory as the AsF_6^- salts.

The basicity of F_5TeNH_2 was previously demonstrated by reaction of F_5TeNH_2 with BF_3 and AsF_5 in CH_2Cl_2 to give the Lewis acid−base adducts, $F_5TeNH_2{\cdot}BF_3$ and $F_5TeNH_2{\cdot}AsF_5$.[14] Only $F_5TeNH_2{\cdot}AsF_5$ is stable to dissociation at room temperature. In view of the established base behavior of F_5TeNH_2, the protonation of F_5TeNH_2 in the superacid medium, HF/AsF_5, and the reactions of XeF_2 with the resulting ammonium salt, $[F_5TeNH_3][AsF_6]$, and of the Lewis acid cation, XeF^+, with F_5TeNH_2 were investigated and are described in the present paper, representing the first synthesis and detailed structural characterization of a noble gas bonded to a formally sp^3-hybridized nitrogen center.

Results and Discussion

Syntheses of F_5TeNH_2, $[F_5TeNH_3][AsF_6]$, and $[F_5TeN(H)Xe][AsF_6]$ and Their ^{15}N-Enriched (99.5%) Analogues: Formation of F_5TeNF_2. (a) F_5TeNH_2, $[F_5TeNH_3][AsF_6]$. Natural abundance and ^{15}N-enriched F_5TeNH_2 compounds were synthesized as previously described (eqs 1 and 2).[14,15] Nitrogen-15 enriched hexamethyldisilazane was prepared according to eqs 3 and 4. The natural abundance and ^{15}N-enriched ammonium salt, $[F_5TeNH_3][AsF_6]$, was prepared and isolated from anhydrous HF in a near quantitative yield according to eq 5 as a moisture-sensitive room-temperature stable salt.

$$TeF_6 + (CH_3)_3SiNHSi(CH_3)_3 \rightarrow F_5TeNHSi(CH_3)_3 + (CH_3)_3SiF \quad (1)$$

$$F_5TeNHSi(CH_3)_3 + HF \rightarrow F_5TeNH_2 + (CH_3)_3SiF \quad (2)$$

$$^{15}NH_4Cl + KOH \rightarrow {}^{15}NH_3 + KCl + H_2O \quad (3)$$

$$3{}^{15}NH_3 + 2(CH_3)_3SiCl \rightarrow 2{}^{15}NH_4Cl + (CH_3)_3Si{}^{15}NHSi(CH_3)_3 \quad (4)$$

$$F_5TeNH_2 + HF + AsF_5 \xrightarrow[HF]{-78 \text{ to } -55\ ^\circ C} [F_5TeNH_3][AsF_6] \quad (5)$$

(b) $[F_5TeN(H)Xe][AsF_6]$. The $F_5TeN(H)Xe^+$ cation was synthesized by reaction of stoichiometric amounts of $[XeF][AsF_6]$ and F_5TeNH_2 in anhydrous HF solvent at −45 to −35 °C according to eqs 6−9. The $[F_5TeN(H)Xe][AsF_6]$ salt was also prepared by reaction of $[F_5TeNH_3][AsF_6]$ with XeF_2 (eq 8) in both anhydrous HF (−45 to −35 °C) and BrF_5 (−62 to −45 °C) solvents. An orange, crystalline solid was deposited from anhydrous HF at −40 °C. The low-temperature Raman spectrum of the solid (−165 °C) was consistent with a mixture of $[F_5TeN(H)Xe][AsF_6]$ (orange), $[F_5TeNH_3][AsF_6]$ (colorless) (eq 8), and $[Xe_2F_3][AsF_6]$ (pale yellow); the latter product resulted from the reaction of XeF_2 with AsF_5 produced in the decomposition of $[F_5TeN(H)Xe][AsF_6]$ (vide infra). Rapid decomposition of $[F_5TeN(H)Xe][AsF_6]$ occurred above −30 °C. Attempts to remove $[F_5TeNH_3][AsF_6]$ and $[Xe_2F_3][AsF_6]$ by washing with HF or by recrystallization resulted in decomposition of the $F_5TeN(H)Xe^+$ cation. The decomposition of $F_5TeN(H)Xe^+$ was shown by ^{19}F NMR spectroscopy (see NMR Spectroscopy) to be complete after several hours at −20 °C and was rapid (ca. 1 min) at −1 °C in HF solution.

$$[XeF][AsF_6] + HF \rightleftharpoons XeF_2 + [H_2F][AsF_6] \quad (6)$$

$$F_5TeNH_2 + [H_2F][AsF_6] \rightarrow [F_5TeNH_3][AsF_6] + HF \quad (7)$$

$$F_5TeNH_2 + (n+2)HF \rightarrow [F_5TeNH_3][HF_2{\cdot}nHF] \quad (8)$$

$$[F_5TeNH_3][AsF_6] + XeF_2 \rightleftharpoons [F_5TeN(H)Xe][AsF_6] + 2HF \quad (9)$$

(c) Decomposition of $[F_5TeN(H)Xe][AsF_6]$ and Formation of F_5TeNF_2. The decomposition of $[F_5TeN(H)Xe][AsF_6]$ in HF solvent was monitored by ^{19}F NMR spectroscopy. An equimolar mixture of $[XeF][AsF_6]$ and F_5TeNH_2 in HF solvent, prepared at −41 °C and warmed to −35 °C for 5 min gave a pale yellow solution. Integration of the ^{19}F NMR resonances at −41 °C gave three major products with molar ratios of $[F_5TeNH_3^+]/[F_5TeN(H)Xe^+]/[TeF_6] = 1.00{:}0.03{:}0.06$ and a trace amount of F_5TeNF_2. The HF solvent resonance at −195.0 ppm ($\Delta\nu_{1/2} = 47$ Hz) and a XeF_2 resonance at −199.8 ppm ($\Delta\nu_{1/2} = 386$ Hz) were also observed. Although the initial reactants were $[XeF][AsF_6]$ and F_5TeNH_2, the absence of a pale yellow precipitate indicative of $[XeF][AsF_6]$ or $[Xe_2F_3][AsF_6]$, which are both sparingly soluble in HF at low temperature,[16] was consistent with the solvolysis of $[XeF][AsF_6]$ (eq 6) and protonation of F_5TeNH_2 (eq 7) leading to XeF_2. Warming the solution to −33 °C over a period of ca. 1 h increased the intensity of the yellow solution and the amounts of orange and pale yellow precipitates. The yellow solution and the orange precipitate are attributed to $[F_5TeN(H)Xe][AsF_6]$, and the pale yellow precipitate is attributed to a mixture of $[Xe_2F_3][AsF_6]$, $[F_5TeN(H)Xe][AsF_6]$, and $[F_5TeNH_3][AsF_6]$ (see Raman Spectroscopy). The ^{19}F NMR spectrum indicated an increased concentration of $F_5TeN(H)Xe^+$ relative to that of $F_5TeNH_3^+$. The formation of $F_5TeN(H)Xe^+$ was also accompanied by decomposition, as indicated by increased amounts of F_5TeNF_2 and TeF_6. The $[F_5TeNH_3^+]/[F_5TeN(H)Xe^+]/[F_5TeNF_2]/[TeF_6]$ molar ratios were $1.00{:}0.26{:}0.02{:}0.28$ after 1 h at −33 °C.

The decomposition of $[F_5TeN(H)Xe][AsF_6]$ in HF to F_5TeNF_2 is consistent with nucleophilic fluorination of F_5TeN-

(9) Emara, A. A. A.; Schrobilgen, G. J. *J. Chem. Soc., Chem. Commun.* **1987**, 1644.
(10) Emara, A. A. A.; Schrobilgen, G. J. *Inorg. Chem.* **1992**, *31*, 1323.
(11) Schrobilgen, G. J. *J. Chem. Soc., Chem. Commun.* **1988**, 1506.
(12) Emara, A. A. A.; Schrobilgen, G. J. *J. Chem. Soc., Chem. Commun.* **1988**, 257.
(13) Schrobilgen, G. J. *J. Chem. Soc., Chem. Commun.* **1988**, 863.
(14) Seppelt, K. *Inorg. Chem.* **1973**, *12*, 2837.
(15) Hartl, H.; Huppman, P.; Lentz. D.; Seppelt, K. *Inorg. Chem.* **1983**, *22*, 2183.
(16) Gillespie, R. J.; Netzer, A.; Schrobilgen, G. J. *Inorg. Chem.* **1974**, *13*, 1455.

Table 1. Summary of Crystal Data and Refinement Results for $[F_5TeNH_3][AsF_6]$, $[F_5TeN(H)Xe][AsF_6]$, and F_5TeNH_2

	$[F_5TeNH_3][AsF_6]$	$[F_5TeN(H)Xe][AsF_6]$	β-F_5TeNH_2	α-F_5TeNH_2
chemical formula	$H_3AsF_{11}NTe$	$HAsF_{11}NTeXe$	H_2F_5NTe	H_2F_5NTe
space group (No.)	$P2_1/m$ (11)	$P\bar{1}$ (2)	$143m$ (217)	$P2_1$ (4)
a (Å)	6.6397(2)	5.3898(3)	6.404(5)	5.163(2)
b (Å)	17.0068(1)	7.0580(3)	6.404(5)	9.083(4)
c (Å)	11.1684(3)	12.5326(4)	6.404(5)	5.262(2)
α (deg)	90	86.736(3)	90	90
β (deg)	105.636(2)	84.064(3)	90	112.223(8)
γ (deg)	90	85.531(3)	90	90
V (Å^3)	1214.47(5)	472.18(4)	262.6(4)	228.4 (2)
molecules/unit cell	6	2	2	2
mol wt (g mol^{-1})	428.55	557.84	238.63	477.25
calcd density (g cm^{-3})	3.516	3.924	3.018	3.469
T (°C)	−109	−109	−5	−113
μ (mm^{-1})	7.889	10.295	5.665	6.512
R_1[a]	0.0271	0.0373	0.0317	0.0413
wR_2[b]	0.0735	0.0946	0.0993	0.1118

[a] R_1 is defined as $\sum||F_o| - |F_c||/\sum|F_o|$ for $I > 2\sigma(I)$. [b] wR_2 is defined as $[\sum[w(F_o^2 - F_c^2)^2]/\sum w(F_o^2)^2]^{1/2}$ for $I > 2\sigma(I)$.

$(H)Xe^+$ accompanied by the liberation of xenon gas ($\delta(^{129}Xe) = -5306$ ppm in HF solvent at −37 °C). Xenon is expected to be a very good leaving group, possibly producing a transient nitrenium ion, F_5TeNH^+, (eq 10). Nucleophilic attack of the nitrenium ion by a fluoride ion donor is expected to result in the monofluoramine F_5TeNHF (eq 11), where the likely fluoride ion donors are HF solvent or AsF_6^-. The enhanced fluoroacidity of the medium that results from the fluorination of F_5TeNH^+ (eq 11) leads to the generation of the strong oxidant cations, XeF^+ and $Xe_2F_3^+$ (eqs 12, 13), which are expected to fluorinate F_5TeNHF to $F_5TeNHF_2^+$ (eq 14) by analogy with similar oxidative fluorinations that have been reported for the reactions of XeF^+ salts with $CF_3S(O)F$, CF_3SSCF_3, H_2S, Cl_2S, and $AsCl_3$ to give $CF_3S(O)F_2^+$,[17] $CF_3SS(F)CF_3^+$,[18] H_2SF^+,[19] Cl_2SF^+,[20] and $AsCl_3F^+$,[21] respectively. As a result of the electron-withdrawing effect of its three highly electronegative ligands and by analogy with NF_3, which is too weakly basic to be protonated in SbF_5/HF solution,[22] $F_5TeNHF_2^+$ is expected to readily deprotonate in HF solvent (eq 15).

The tellurium hexafluoride observed in the decomposition was shown to come from the reaction of HF with $F_5TeNH_3^+$ (eq 16). The ^{19}F and ^1H NMR spectra of F_5TeNH_2 in HF solvent at −33 °C showed the presence of $F_5TeNH_3^+$ and TeF_6 in a $[F_5TeNH_3^+]/[TeF_6]$ molar ratio of 1.00:0.08, and a 1:1:1 triplet in the ^1H NMR spectrum at $\delta(^1H) = 5.67$ ppm $[^1J(^1H\text{-}^{14}N) = 54$ Hz] indicated the presence of NH_4^+.[22,23]

$$F_5TeN(H)Xe^+ \rightarrow [F_5TeNH^+] + Xe \quad (10)$$

$$[F_5TeNH^+] + 2HF/AsF_6^- \rightarrow F_5TeNHF + H_2F^+/AsF_5 \quad (11)$$

$$AsF_5 + XeF_2 \rightleftharpoons XeF^+AsF_6^- \quad (12)$$

$$[XeF][AsF_6] + XeF_2 \rightleftharpoons [Xe_2F_3][AsF_6] \quad (13)$$

$$F_5TeNHF + XeF^+(Xe_2F_3^+) \rightarrow F_5TeNHF_2^+ + Xe(Xe + XeF_2) \quad (14)$$

$$F_5TeNHF_2^+ + HF \rightarrow F_5TeNF_2 + H_2F^+ \quad (15)$$

$$[F_5TeNH_3][AsF_6]/[HF_2\cdot nHF] + HF \rightarrow TeF_6 + [NH_4][AsF_6]/[HF_2\cdot nHF] \quad (16)$$

X-ray Crystal Structures of F_5TeNH_2, $[F_5TeNH_3][AsF_6]$ and $[F_5TeN(H)Xe][AsF_6]$. A summary of the refinement results and other crystallographic information are provided in Table 1. Important bond lengths and angles for F_5TeNH_2, $[F_5TeN(H)Xe][AsF_6]$, and $[F_5TeNH_3][AsF_6]$ are listed in Tables 2 and S1 along with the calculated values. Only the geometrical parameters for the ordered low-temperature α-phase of F_5TeNH_2 are compared.

The values related to $[F_5TeNH_3][AsF_6]$ and F_5TeNH_2 are given in square brackets and braces, respectively. The tellurium environments in all three structures are pseudooctahedral with Te−N (1.982(5)), [2.043(3), 2.049(3)], {1.94(2)} Å) and Te−F (average, 1.807(4), [1.814(2)], {1.85(4)} Å) bond lengths comparable to those reported for $F_5TeN{=}NCl_4$[15] and F_5TeNCO.[24]

(a) $[F_5TeNH_3][AsF_6]$. The structure of $[F_5TeNH_3][AsF_6]$ (Figure 1) consists of well-separated $F_5TeNH_3^+$ cations and AsF_6^- anions. The closest intra- and intermolecular N···F contacts range from 2.707 to 2.909 Å and are within the sum of their van der Waals radii (NH_4^+, 1.51 Å; F, 1.47 Å),[25] but they do not affect the geometry of the octahedral AsF_6^- anion.

(b) F_5TeNH_2. The arrangements of F_5TeNH_2 molecules in the lattices of their low-temperature (α) and high-temperature (β) phases are illustrated in Figure 2a and Figure 2b, respectively. Each molecule in β-F_5TeNH_2 is surrounded by eight molecules (5.546 Å) occupying the corners of a cube, while in the structure of α-F_5TeNH_2, each molecule is also surrounded by eight molecules with six of them occupying the corners of an irregular hexagon at Te···Te distances of 5.226 (×2), 5.262 (×2), and 5.282 (×2) Å and two at Te···Te distances of 5.163 Å above and below the hexagonal plane. The closest intermolecular contacts observed for α-F_5TeNH_2 are N(1)···F(3A) = 3.076 Å and

(17) Minkwitz, R.; Molsbeck, W. *Z. Anorg. Allg. Chem.* **1992**, *612*, 35.
(18) Minkwitz, R.; Nowicki, G. *Inorg. Chem.* **1991**, *30*, 4426.
(19) Minkwitz, R.; Nowicki, G.; Bäck, B.; Sawodny, W. *Inorg. Chem.* **1993**, *32*, 787.
(20) Minkwitz, R.; Nowicki, G. *Z. Naturforsch.* **1989**, *44b*, 1343.
(21) Minkwitz, R.; Molsbeck, W. *Z. Anorg. Allg. Chem.* **1992**, *607*, 175.
(22) Christe, K. O. *Inorg. Chem.* **1975**, *14*, 2821.
(23) Mason, J.; Christe, K. O. *Inorg. Chem.* **1983**, *22*, 1849.
(24) Seppelt, K.; Oberhammer, H. *Inorg. Chem.* **1985**, *24*, 1227.
(25) Bondi, A. *J. Phys. Chem.* **1964**, *68*, 441.

Table 2. Experimental Geometries for $[F_5TeNH_3][AsF_6]$, $[F_5TeN(H)Xe][AsF_6]$, and F_5TeNH_2 and Calculated Geometries for $F_5TeNH_3^+$, $F_5TeN(H)Xe^+$, F_5TeNH_2, and F_5TeNF_2

$[F_5TeNH_3][AsF_6]$[a]

bond lengths (Å)

	exptl		exptl	DFT	HF
Te(1)−N(1)	2.049(3)	Te(2)−N(2)	2.043(2)	2.056	2.094
Te(1)−F(1)	1.810(2)	Te(2)−F(8)	1.806(2)	1.774	1.758
Te(1)−F(2)	1.814(2)	Te(2)−F(6)	1.819(2)	1.796	1.780
Te(1)−F(2A)	1.814(2)	Te(2)−F(4)	1.815(2)	1.797	1.780
Te(1)−F(3)	1.815(2)	Te(2)−F(5)	1.819(2)	1.795	1.780
Te(1)−F(3A)	1.815(2)	Te(2)−F(7)	1.815(2)	1.796	1.780

bond angles (deg)

	exptl		exptl	DFT	HF
F(1)−Te(1)−F(2)	91.33(8)	F(6)−Te(2)−F(8)	90.57(8)	94.2	94.2
F(1)−Te(1)−F(2A)	91.32(8)	F(4)−Te(2)−F(8)	91.70(9)	93.2	94.2
F(1)−Te(1)−F(3)	91.29(8)	F(5)−Te(2)−F(8)	90.72(9)	93.4	94.3
F(1)−Te(1)−F(3A)	91.29(8)	F(7)−Te(2)−F(8)	90.75(8)	93.6	94.2
F(1)−Te(1)−N(1)	179.77(11)	F(8)−Te(2)−N(2)	179.07(8)	179.4	179.5
F(2)−Te(1)−F(2A)	90.57(12)	F(4)−Te(2)−F(6)	90.20(8)	89.5	89.6
F(2)−Te(1)−F(3)	89.28(9)	F(5)−Te(2)−F(6)	89.55(8)	90.1	89.8
F(2)−Te(1)−F(3A)	177.39(8)	F(6)−Te(2)−F(7)	178.59(7)	172.1	171.6
F(2)−Te(1)−N(1)	88.84(9)	F(6)−Te(2)−N(2)	89.75(8)	86.3	85.7
F(3)−Te(1)−F(2A)	177.39(8)	F(4)−Te(2)−F(5)	177.57(7)	173.3	171.5
F(3)−Te(1)−F(3A)	90.75(12)	F(5)−Te(2)−F(7)	89.94(8)	89.6	89.8
F(3)−Te(1)−N(1)	88.55(9)	F(5)−Te(2)−N(2)	88.41(9)	86.3	85.2
F(2A)−Te(1)−F(3A)	89.28(9)	F(4)−Te(2)−F(7)	90.26(8)	89.6	89.6
F(2A)−Te(1)−N(1)	88.84(9)	F(4)−Te(2)−N(2)	89.17(10)	87.1	86.3
F(3A)−Te(1)−N(1)	88.55(9)	F(7)−Te(2)−N(2)	88.92(8)	85.9	85.8

$[F_5TeN(H)Xe][AsF_6]$[b]

bond lengths (Å)

	exptl	DFT	HF		exptl	DFT	HF
Te(1)−N(1)	1.982(5)	2.002	2.036	Te(1)−F(5)	1.801(4)	1.791	1.778
Te(1)−F(1)	1.791(4)	1.780	1.765	N(1)−H(1)	0.93(6)	1.045	1.011
Te(1)−F(2)	1.805(4)	1.811	1.794	Xe(1)−N(1)	2.044(4)	1.986	2.067
Te(1)−F(3)	1.819(3)	1.803	1.786	Xe(1)−F(11)	2.580(3)		
Te(1)−F(4)	1.820(3)	1.811	1.789	F(11)−As(1)	1.740(4)		

bond angles (deg)

	exptl	DFT	HF		exptl	DFT	HF
F(1)−Te(1)−F(2)	88.8(2)	90.3	90.6	F(3)−Te(1)−F(5)	89.6(2)	90.6	90.3
F(1)−Te(1)−F(3)	89.6(2)	93.5	93.6	F(3)−Te(1)−N(1)	88.8(2)	83.8	85.7
F(1)−Te(1)−F(4)	91.5(2)	93.7	93.3	F(4)−Te(1)−F(5)	90.4(2)	89.7	90.5
F(1)−Te(1)−F(5)	88.4(2)	91.0	91.7	F(4)−Te(1)−N(1)	90.1(2)	89.0	87.5
F(1)−Te(1)−N(1)	176.6(2)	177.2	179.1	F(5)−Te(1)−N(1)	88.6(2)	88.2	87.8
F(2)−Te(1)−F(3)	90.4(2)	90.6	90.2	Te(1)−N(1)−Xe(1)	115.1(2)	115.9	137.6
F(2)−Te(1)−F(4)	89.7(2)	89.0	88.7	Te(1)−N(1)−H(1)	109(4)	108.6	112.9
F(2)−Te(1)−F(5)	177.2(2)	178.2	177.7	Xe(1)−N(1)−H(1)	107(4)	105.9	104.3
F(2)−Te(1)−N(1)	94.2(2)	90.6	90.0	F(11)−Xe(1)−N(1)	171.6(2)		
F(3)−Te(1)−F(4)	178.9(2)	172.7	173.1	As(1)−F(11)−Xe(1)	128.1(2)		

α-F_5TeNH_2 (−113 °C)[c]

bond lengths (Å)

	exptl	DFT	HF		exptl	DFT	HF
Te(1)−N(1)	1.96(2)	1.876	1.907	Te(1)−F(3)	1.85(2)	1.818	1.805
Te(1)−F(1)	1.83(1)	1.813	1.793	Te(1)−F(4)	1.84(2)	1.818	1.805
Te(1)−F(2)	1.854(6)	1.831	1.812	Te(1)−F(5)	1.854(6)	1.812	1.799

bond angles (deg)

	exptl	DFT	HF		exptl	DFT	HF
F(1)−Te(1)−F(2)	88.1(7)	85.1	85.7	F(2)−Te(1)−N(1)	94.7(9)	95.3	94.6
F(1)−Te(1)−F(3)	85.5(3)	89.7	89.2	F(3)−Te(1)−F(4)	174.4(10)	179.3	178.5
F(1)−Te(1)−F(4)	89.0(10)	89.7	89.2	F(3)−Te(1)−F(5)	90.1(8)	89.8	90.1
F(1)−Te(1)−F(5)	86.1(7)	86.4	86.2	F(3)−Te(1)−N(1)	89.3(10)	90.3	90.8
F(1)−Te(1)−N(1)	174.0(10)	179.6	179.7	F(4)−Te(1)−F(5)	90.4(8)	89.8	90.1
F(2)−Te(1)−F(3)	88.3(8)	90.2	89.8	F(4)−Te(1)−N(1)	96.3(3)	90.3	90.8
F(2)−Te(1)−F(4)	90.6(8)	90.2	89.8	F(5)−Te(1)−N(1)	91.0(10)	93.2	93.5
F(2)−Te(1)−F(5)	174.1(7)	171.5	171.9				

Table 2. Continued

F_5TeNF_2[d]

bond lengths (Å)						bond angles (deg)					
	DFT	HF		DFT	HF		DFT	HF		DFT	HF
Te−N	2.099	2.049	$Te-F_e$	1.819	1.794	F_a-Te-F_e	89.7	89.4	F_e-Te-F_e	90.3	90.7
$Te-F_e$	1.816	1.793	$Te-F_e$	1.824	1.797	F_a-Te-F_e	89.8	89.7	F_e-Te-F_e	179.2	179.2
$Te-F_e$	1.819	1.794	$Te-F_a$	1.803	1.782	F_a-Te-F_e	89.8	89.7	F_e-Te-F_e	179.2	178.5
N−F × 2	1.378	1.343				F_a-Te-F_e	89.8	89.8	F_e-Te-F_e	89.7	89.3
						F_a-Te-N	178.4	178.6	F_e-Te-F_e	89.7	89.3
						F_e-Te-N	90.2	90.3	F_e-Te-F_e	90.3	90.7
						F_e-Te-N	90.2	90.3	Te−N−F ×2	102.9	106.3
						F_e-Te-N	88.5	89.1	F−N−F	103.7	103.4
						F_e-Te-N	92.0	91.8			

F_5TeN^{2-}[d]

bond lengths (Å)				bond angles (deg)			
	DFT		DFT		DFT		DFT
Te−N	1.753	$Te-F_a$	1.936	F_a-Te-F_e	89.7	F_e-Te-N	90.3
$Te-F_e$	1.970						

[a] Other bond lengths (Å) and bond angles (deg) for $F_5TeNH_3^+$: N(1)−H and N(2)−H exptl 0.821, 0.833, calcd 1.042 (DFT), 1.014 (HF); Te(1)−N(1)−H and Te(2)−N(2)−H exptl 110.1, 109.5, calcd 109.4, 110.3, 109.9 (DFT), 110.9, 110.7, 110.7 (HF); H−N(1)−H and H−N(2)−H exptl 108.8, 108.9, 109.5, calcd 109.0, 109.0, 109.3 (DFT), 108.1, 108.1, 108.1 (HF). [b] Calculated values correspond to the isolated $F_5TeN(H)Xe^+$ cation. [c] Other bond lengths (Å) and bond angles (deg) for F_5TeNH_2: N(1)−H exptl 0.896, calcd 1.028 (DFT), 1.000 (HF); Te(1)−N(1)−H exptl 99.4, 107.7, calcd 112.0 (DFT), 113.9(HF); H−N(1)−H exptl 128.1, calcd 112.3 (DFT), 112.9 (HF). [d] The labels correspond to those used in Structure IV (F_5TeNF_2).

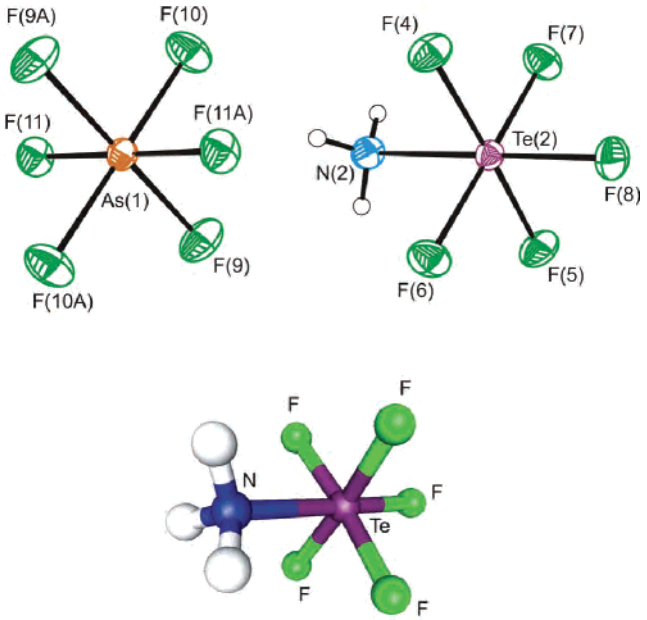

Figure 1. X-ray crystal structure of $[F_5TeNH_3][AsF_6]$ (top); thermal ellipsoids are shown at the 50% probability level. Calculated geometry of the $F_5TeNH_3^+$ cation (bottom).

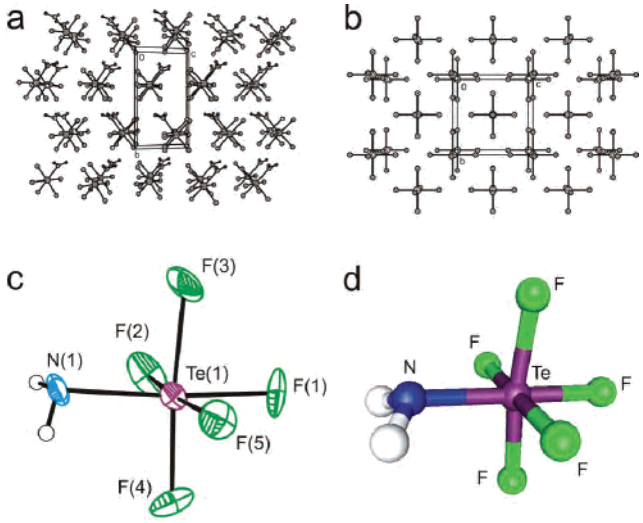

Figure 2. View of the F_5TeNH_2 unit cell along the *c* axis at (a) −113 and (b) −5 °C. (c) X-ray crystal structure of F_5TeNH_2 at −113 °C; thermal ellipsoids are shown at the 50% probability level. (d) Calculated geometry of F_5TeNH_2.

N(1)···F(6A) = 3.020 Å, which are at the limit of the sum of the van der Waals radii for NH_4^+ and F. The Te−F/N bond length (1.82(2) Å) in β-F_5TeNH_2 is within $\pm 3\sigma$ of the average value of the Te−F and Te−N bond lengths in α-F_5-$TeNH_2$ (Figure 2c).

(c) $[F_5TeN(H)Xe][AsF_6]$. The $F_5TeN(H)Xe^+$ cation and the AsF_6^- anion form an ion pair by interaction through a Xe···F−As fluorine bridge (Figure 3). The Xe−N bond length (2.044(4) Å) is comparable to that observed in $[XeN(SO_2F)_2][Sb_3F_{16}]$ (2.02(1) Å)[5] but is significantly shorter than that in $FXeN(SO_2F)_2$ (2.200(3) Å).[2] Each AsF_6^- anion in $[F_5TeN(H)Xe][AsF_6]$ is fluorine-bridged to a single $F_5TeN(H)Xe^+$ cation through a Xe···F bridge bond (vide infra). As a result, the AsF_6^- anion in $[F_5TeN(H)Xe][AsF_6]$ has a distorted octahedral geometry, giving an As−F bridge bond length (1.740(4) Å) that is significantly longer than the others (average, 1.696(4) Å). Similar lengthenings of the As−F bridge bonds in the AsF_6^- anions occur in $HF\cdot[HO-TeF_4-O-Xe][AsF_6]$ (1.771(7) Å),[26] $[XeF][AsF_6]$ (1.813(6) Å),[27] $[KrF][AsF_6]$ (1.845(2) Å),[28] $[Kr_2F_3][AsF_6]\cdot[KrF][AsF_6]$ (1.878(6) Å),[28] and $[C_6F_5Xe][AsF_6]$ (1.743(4), 1.748(3) Å)[29] where one of the fluorine atoms of the AsF_6^- anion is also coordinated to a noble gas atom. The Xe···F bridge bond

(26) Turowsky, L.; Seppelt, K. *Inorg. Chem.* **1990**, *29*, 3226.
(27) Zalkin, A.; Ward, D. L.; Biagioni, R. N.; Templeton, D. H.; Bartlett, N. *Inorg. Chem.* **1978**, *17*, 1318.
(28) Lehmann, J. F.; Dixon, D. A.; Schrobilgen, G. J. *Inorg. Chem.* **2001**, *40*, 3002.
(29) Frohn, H.-J.; Klose, A.; Schroer, T.; Henkel, G.; Buss, V.; Opitz, D.; Vahrenhorst, R. *Inorg. Chem.* **1998**, *37*, 4884.

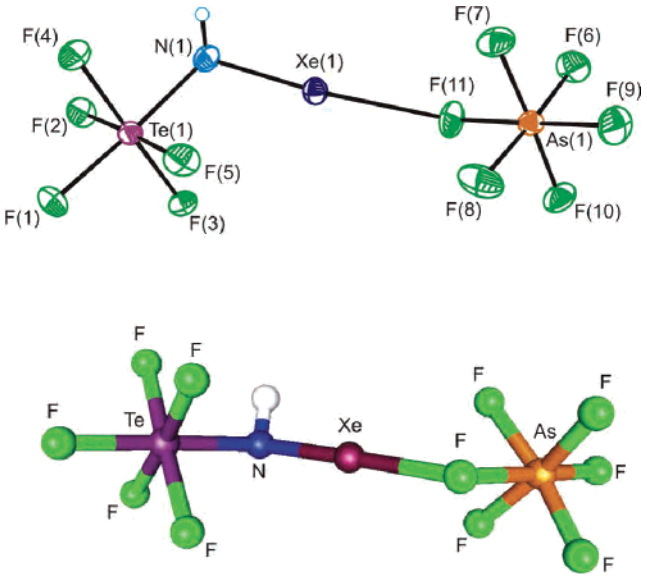

Figure 3. X-ray crystal structure of $[F_5TeN(H)Xe][AsF_6]$ (top); thermal ellipsoids are shown at the 50% probability level. Calculated geometry of the $[F_5TeN(H)Xe][AsF_6]$ ion pair (bottom).

(2.580(3) Å) is significantly shorter than the sum of the xenon and fluorine (3.63 Å)[25] van der Waals radii but is significantly longer than the terminal Xe−F bond in $FXeN(SO_2F)_2$ (1.967(3) Å)[2] and the bridging Xe···F bond distances in $[XeN(SO_2F)_2][Sb_3F_{16}]$ (2.457(8) Å)[5] and $[XeF][AsF_6]$ (2.212(5) Å).[27]

The Xe, Te, and H atoms in $[F_5TeN(H)Xe][AsF_6]$ form a near-tetrahedral (sp^3-hybridized) arrangement about nitrogen having a bond angle sum (331.1(3)°) that is only slightly larger than the sum of the ideal tetrahedral angles (3 × 109.5° = 328.5°), whereas the $XeNS_2$ arrangements in $FXeN(SO_2F)_2$[2] and $[XeN(SO_2F)_2][Sb_3F_{16}]$[5] are planar ($sp^2$-hybridized) having bond angle sums of 359.9 and 359.6°, respectively.

The N−Xe···F angle (171.6(2)°) in $[F_5TeN(H)Xe][AsF_6]$ is significantly less than that previously reported for $[XeN(SO_2F)_2][Sb_3F_{16}]$ (178.3(3)°).[5] The distortion from linearity appears to be inconsistent with a linear AX_2E_3 VSEPR arrangement and may result from several fluorine contacts to xenon (Xe···F(4) = 3.169 Å, Xe···F(11A) = 3.281 Å, Xe···F(8B) = 3.265 Å, and Xe···F(10E) = 3.260 Å) which are within the sum of fluorine and xenon van der Waals radii and avoid the electron lone pairs of xenon. Similar deviations from linearity are, however, also obtained for the energy-minimized gas-phase geometries (see Computational Results) and therefore may not be attributable to packing effects alone. The Ng···F−As (Ng = Xe, Kr) bridge bond angle of 128.1(2)° is comparable to those in $[XeF][AsF_6]$ (134.8(2)°),[27] HF·$[HO-TeF_4-OXe][AsF_6]$ (133.0(4)°),[26] $[KrF][AsF_6]$ (133.7(1)°),[28] and $[Kr_2F_3][AsF_6]$·$[KrF][AsF_6]$ (127.5(3)°)[28] and is consistent with an AX_2E_2 VSEPR arrangement and the bent geometry predicted by this model. The observed range of the Xe···F−As and Kr···F−As angles shows that this angle is very much influenced by crystal packing.

NMR Spectroscopy. The ^1H, ^{15}N, ^{19}F, ^{125}Te, and ^{129}Xe NMR parameters for F_5TeNH_2, $[F_5TeNH_3][AsF_6]$, $[F_5TeN(H)Xe][AsF_6]$, and F_5TeNF_2 (Structures I−IV) are listed in Table 3.

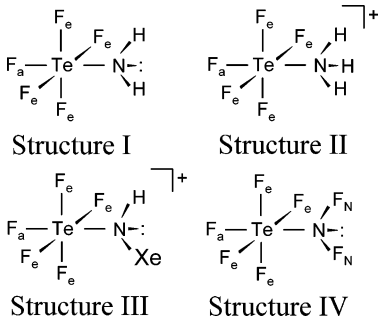

Couplings with ^{14}N ($I = 1$) were not observed for any of the natural abundance species studied because of rapid quadrupolar relaxation of the ^{14}N spin states caused by the nonzero electric-field gradients at the ^{14}N nuclei of these compounds; consequently, the spectra of the 99.5% ^{15}N-enriched compounds ($I = {}^1/_2$) were obtained.

(a) F_5TeNH_2 and $[^{15}N]F_5TeNH_2$. The ^{19}F and ^1H NMR spectra of natural abundance F_5TeNH_2 have been previously reported in CH_2Cl_2 solvent at room temperature.[14] The only parameters reported then were $\delta(^{19}F_{a,e})$, $\delta(^1H)$, $^1J(^{19}F_e-^{19}F_a)$, and $^1J(^{125}Te-^{19}F_{a,e})$, which are in good agreement with those obtained in the present study (Table 3). A fuller solution characterization by ^{15}N, ^1H, ^{19}F, and ^{125}Te NMR spectroscopy of the natural abundance and ^{15}N-enriched compounds is provided in Table 3.

(b) $[F_5TeNH_3][AsF_6]$ and $[^{15}N][F_5TeNH_3][AsF_6]$. The ^1H NMR spectrum of $[F_5TeNH_3][AsF_6]$ in BrF_5 solvent at −53 °C (Figure S1a) consists of a broad singlet centered at 7.45 ppm ($\Delta\nu_{1/2}$ = 28 Hz). The broadening and absence of resolved couplings results from fast quadrupolar relaxation by the directly bonded ^{14}N atom. The ^1H NMR spectrum of $[^{15}N][F_5TeNH_3][AsF_6]$ in BrF_5 solvent at −56 °C (Figure S1b) is a doublet (7.43 ppm) resulting from $^1J(^{15}N-^1H)$ = 76 Hz, which is accompanied by ^{125}Te satellites resulting from $^2J(^{125}Te-^1H)$ = 25 Hz.

The ^{19}F NMR spectrum of $[F_5TeNH_3][AsF_6]$ at −44 °C in BrF_5 solvent (Figure S2) is an AB_4 spin pattern resulting from the pseudo-octahedral F_5TeN group, which is accompanied by ^{125}Te satellites from $^1J(^{125}Te-^{19}F_a)$ and $^1J(^{125}Te-^{19}F_e)$. The assignments of the chemical shifts and coupling constants were made by analogy with those of F_5TeNH_2 (Table 3). A resonance at −60 ppm, which is broadened ($\Delta\nu_{1/2}$ = 770 Hz) by quadrupolar relaxation of ^{75}As ($I = {}^3/_2$), is assigned to the AsF_6^- anion. A weak peak at −53.2 ppm is assigned to TeF_6, which results from solvent attack, and a broad, weak resonance at −52.0 ppm is also attributed to an unknown solvolysis product.

The ^{15}N NMR spectrum of $[^{15}N][F_5TeNH_3][AsF_6]$ (Figure S3) at −40 °C in HF solvent consists of a quartet centered at −317.1 ppm results from $^1J(^{15}N-^1H)$ = 76 Hz (the calculated $^1J(^{14}N-^1H)$ value is 54 Hz), and is in agreement with the value obtained from the ^1H NMR spectrum. Each quartet line is flanked by ^{125}Te satellites resulting from $^1J(^{125}Te-^{15}N)$ = 48 Hz which is in good agreement with the value

Table 3. NMR Chemical Shifts and Spin−Spin Coupling Constants for F_5TeNH_2, F_5TeNF_2, $[F_5TeNH_3][AsF_6]$, and $[F_5TeN(H)Xe][AsF_6]$[a]

F_5TeNH_2 [b]					F_5TeNF_2				
chemical shifts (ppm)		T (°C)	coupling constants (Hz)		chemical shifts (ppm)		T (°C)	coupling constants (Hz)	
$\delta(^{125}Te)$	683.8		$^1J(^{125}Te-^{19}F_a)$	3284	$\delta(^{19}F_{Te})$	[−57.0], F_a	[−60]	$^2J(^{19}F_a-^{19}F_e)$	[148]
			$^1J(^{123}Te-^{19}F_e)$	2944		[−59.5], F_e			
			$^1J(^{125}Te-^{19}F_e)$	3519	$\delta(^{19}F_N)$	[64.2]	[−60]	$^1J(^{19}F_N-^{15}N)$	[165]
	−37.3, F_a	27	$^2J(^{19}F_a-^{19}F_e)$	169.8				$^2J(^{125}Te-^{19}F_N)$	[1025]
	−42.8, F_e							$^3J(^{19}F_N-^{19}F_e)$	[15]
$\delta(^{15}N)$	−312.0	27	$^1J(^{125}Te-^{15}N)$	231.2	$\delta(^{15}N)$	[−11.1]	[−57]	$^2J(^{19}F_e-^{15}N)$	[11]
			$^1J(^{19}F_e-^{15}N)$	5.4					
$\delta(^1H)$	4.30	27	$^1J(^{15}N-^1H)$	71.0					
			$^2J(^{125}Te-^1H)$	41.8					

$[F_5TeNH_3][AsF_6]$[c]					$[F_5TeN(H)Xe][AsF_6]$[d]				
chemical shifts (ppm)		T (°C)	coupling constants (Hz)		chemical shifts (ppm)		T (°C)	coupling constants (Hz)	
$\delta(^{125}Te)$	588[e]	−45[e]	$^1J(^{125}Te-^{19}F_a)$	3801[e]	$\delta(^{129}Xe)$	−2841 [−2902][e]	−39 [−45][e]	$^1J(^{129}Xe-^{15}N)$	138 [142][e]
			$^1J(^{125}Te-^{19}F_e)$	3651[e]				$^2J(^{129}Xe-^1H)$	24
			$^1J(^{123}Te-^{19}F_e)$	[3024]				$^3J(^{129}Xe-^{19}F_e)$	6
$\delta(^{19}F)$	[−55.6], F_a	[−44]	$^2J(^{19}F_a-^{19}F_e)$	[162]	$\delta(^{125}Te)$	598[e]	−34[e]	$^1J(^{125}Te-^{19}F_a)$	3578[e]
	[−30.2], F_e							$^1J(^{125}Te-^{19}F_e)$	3766[e]
$\delta(^{15}N)$	−317.1[e]	−40[e]	$^1J(^{125}Te-^{15}N)$	48[e]				$^1J(^{123}Te-^{19}F_e)$	[3113]
					$\delta(^{19}F)$	−51.6 [−51.9], F_a	−31 [−44]	$^2J(^{19}F_a-^{19}F_e)$	166
$\delta(^1H)$	[7.43][e]	[−53][e]	$^1J(^{15}N-^1H)$	[76][e]		−43.4 [−43.2], F_e			
			$^2J(^{125}Te-^1H)$	25[e]	$\delta(^{15}N)$	−268.0[e] [−266.3][e]	−40[e] [−45][e]	$^1J(^{125}Te-^{15}N)$	333[e]
					$\delta(^1H)$	[6.90]	[−44]	$^1J(^{15}N-^1H)$	62[e][62][e]
								$^2J(^{125}Te-^1H)$	46[e][46]

[a] The values in square brackets have been measured in BrF_5 solvent; all other values have been measured in HF solvent unless otherwise specified. The axial and equatorial fluorines of the TeF_5 groups are denoted by F_a and F_e, respectively. [b] Recorded in CD_2Cl_2 solvent. Previously reported NMR parameters were obtained for F_5TeNH_2 in CH_2Cl_2 at room temperature are from ref 14: $\delta(^{19}F_a) = -37.2$ ppm, $\delta(^{19}F_e) = -43.2$ ppm, $^2J(^{19}F_a-^{19}F_e) = 176$ Hz, $^1J(^{125}Te-^{19}F_a) = 3290$ Hz, $^1J(^{125}Te-^{19}F_e) = 3565$ Hz, and $\delta(^1H) = 4.80$ ppm. [c] The ^{19}F spectrum in HF solvent at −44 °C displayed a broad saddle-shaped feature at −68 ppm from the partially quadrupole-collapsed coupling, $^1J(^{75}As-^{19}F)$, of the octahedral AsF_6^- anion, whereas in BrF_5 solvent, the AsF_6^- resonance at −60 ppm was quadrupole collapsed into a broad singlet. The ^{19}F and ^{125}Te NMR parameters for the decomposition product, TeF_6, are $\delta(^{19}F) = -56.6$ ppm, $\delta(^{125}Te) = 524.2$ ppm, $^1J(^{125}Te-^{19}F) = 3723$ Hz, and $^1J(^{123}Te-^{19}F) = 3088$ Hz in HF at −31 °C and $\delta(^{19}F) = -56.5$ ppm, $^1J(^{125}Te-^{19}F) = 3732$ Hz, and $^1J(^{123}Te-^{19}F) = 3091$ Hz in BrF_5 at −44 °C. [d] The ^{19}F spectra in HF and BrF_5 solvents displayed a broad feature at −68 and −63 ppm, respectively, assigned to the partially quadrupole-collapsed $^1J(^{75}As-^{19}F)$ coupling of the octahedral AsF_6^- anion. [e] Obtained from a 99.5% ^{15}N-enriched sample of $[F_5TeN(H)Xe][AsF_6]$ or $[F_5TeNH_3][AsF_6]$.

obtained from the ^{125}Te NMR spectrum. The magnitude of the one-bond reduced N−H coupling constant is comparable to that observed for related compounds containing formally sp^3-hybridized and positively charged nitrogen centers (cf. NH_4^+,[23] $^1J(^{14}N-^1H) = 54.3$ Hz; $CH_3NH_3^+$,[30] $^1J(^{15}N-^1H) = 75.6$ Hz, calculated $^1J(^{14}N-^1H) = 54.9$ Hz).

The ^{125}Te NMR chemical shift ($\delta(^{125}Te) = 588$ ppm) of $[^{15}N][F_5TeNH_3][AsF_6]$ in HF solvent at −45 °C (Figure S4) is consistent with that expected for the F_5Te- group (cf. F_5TeOH, $\delta(^{125}Te) = 601$ ppm in CH_3CN solvent).[31] All possible J-couplings involving ^{125}Te were observed (Table 3). The ^{125}Te NMR resonance is split into a doublet, from the one-bond coupling $^1J(^{125}Te-^{19}F_a) = 3801$ Hz, which, in turn, is split into a quintet by coupling of tellurium to four equivalent equatorial fluorines ($^1J(^{125}Te-^{19}F_e) = 3651$ Hz). Both couplings are in agreement with those observed in the ^{19}F NMR spectra. Each line of the doublet of quintets is also split into a doublet of quartets by coupling of ^{125}Te to ^{15}N ($^1J(^{125}Te-^{15}N) = 48$ Hz) and to the three equivalent protons of the H_3N group ($^2J(^{125}Te-^1H) = 25$ Hz). The magnitude of $^2J(^{125}Te-^1H)$ is in agreement with that obtained from the ^1H NMR spectrum and its observation, along with the observation of $^1J(^{15}N-^1H)$, indicates that the proton exchange rate between $F_5TeNH_3^+$ and the HF solvent is slow on the NMR time scale.

(c) $[F_5TeN(H)Xe][AsF_6]$ and $[^{15}N][F_5TeN(H)Xe][AsF_6]$. The NMR spectroscopic findings in HF and BrF_5 solvents are consistent with eq 6−9 and 16. Consequently, resonances resulting from the $F_5TeNH_3^+$ cation, XeF_2, and TeF_6 (HF solvent) (Table 3) were also observed, as well as trace amounts of F_5TeNF_2 (vide infra).

The ^{19}F NMR spectra of $F_5TeN(H)Xe^+$ in HF solvent at −31 °C (Figure 4) and in BrF_5 solvent at −44 °C consist of AX_4 patterns at −51.6 and −51.9 ppm (A) and −43.4 and −43.2 ppm (X_4), respectively (see Table 3 and Decomposition of $[F_5TeN(H)Xe][AsF_6]$ and Formation of F_5TeNF_2). Of the four possible natural abundance ^{19}F couplings to ^{123,125}-Te, satellites resulting from $^1J(^{125}Te-^{19}F_a)$, $^1J(^{125}Te-^{19}F_e)$, and $^1J(^{123}Te-^{19}F_e)$, were observed. The broad, saddle-shaped resonance at −68 ppm ($\Delta\nu_{1/2} = 2588$ Hz) in HF solvent (−31 °C) was assigned to the partially quadrupole-collapsed $^1J(^{75}As-^{19}F)$ 1:1:1:1 quartet of the AsF_6^- anion. The ^{19}F resonance of the AsF_6^- anion in BrF_5 solvent was also observed at −63 ppm (Table 3) and is a single, broad ($\Delta\nu_{1/2}$, 617 Hz), quadrupole-collapsed line.

At initial XeF_2 and $[F_5TeNH_3][AsF_6]$ concentrations of 0.38 and 0.36 M, respectively, in BrF_5 solvent at −60 °C, the relative concentrations of $[F_5TeNH_3^+]$/ $[F_5TeN(H)Xe^+]$ were 1.0:1.2 based on integration of the ^{19}F NMR spectrum after warming the sample to −40 °C for 10 min. The

(30) Binsch, G.; Lambert, J. B.; Roberts, B. W.; Roberts, J. D. *J. Am. Chem. Soc.* **1964**, *86*, 5564.
(31) Tötsch, W.; Peringer, P.; Sladky, F. *J. Chem. Soc., Chem. Commun.* **1981**, 841.

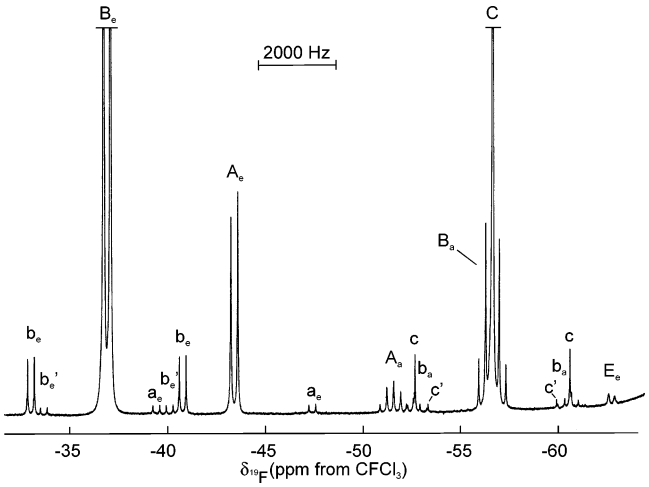

Figure 4. ^{19}F NMR spectrum (470.599 MHz) of the fluorine-on-tellurium-(VI) region of an equimolar mixture of natural abundance F_5TeNH_2 and $[XeF][AsF_6]$ in HF solvent, warmed to −35 °C for 5 min prior to recording the spectrum at −31 °C: (A_e) equatorial fluorine resonance of $F_5TeN(H)Xe^+$ and ^{125}Te (a_e) satellites, (A_a) axial fluorine resonance of $F_5TeN(H)Xe^+$, (B_e) equatorial fluorine resonance of $F_5TeNH_3^+$ and ^{125}Te (b_e) and ^{123}Te (b_e') satellites, (B_a) axial fluorine resonance of $F_5TeNH_3^+$ and ^{125}Te (b_a) satellites, (C) overlapping resonances of TeF_6 and central quintet line of the axial fluorine of $F_5TeNH_3^+$ (B_a) and ^{125}Te (c) and ^{123}Te (c′) satellites, and (E_e) equatorial fluorine-on-tellurium resonance of F_5TeNF_2.

equilibrium ratio was 1.0:0.3 when initial $[XeF][AsF_6]$ and F_5TeNH_2 concentrations of 0.71 M in HF solvent at −33 °C were used. The lower relative amount of $F_5TeN(H)Xe^+$ in HF solvent is attributed to suppression of the HF elimination reaction (eq 9) by anhydrous HF solvent. The observation of XeF_2 in the ^{19}F and ^{129}Xe NMR spectra is also in accordance with eq 9. The XeF_2 resonance in the ^{19}F NMR spectrum in BrF_5 solvent was observed at −184.1 ppm ($^1J(^{129}Xe-^{19}F) = 5621$ Hz) along with a doublet assigned to HF at −192.8 ppm ($^1J(^{19}F-^1H) = 527$ Hz).

The ^{129}Xe NMR spectrum of natural abundance $F_5TeN(H)Xe^+$ consists of a broad singlet at −2841 ppm in HF solvent (−45 °C; Figure 5a) and at −2902 ppm in BrF_5 solvent (−48 °C). On the basis of its high ^{129}Xe shielding, $F_5TeN(H)Xe^+$ may be classified as one of the most covalent bonds formed by xenon.[32] The ^{129}Xe shielding is similar to those in $F_5SN(H)Xe^+$ (−2886 ppm, HF solvent, −20 °C) and $F_4S{=}NXe^+$ (−2672 ppm, HF, −20 °C)[32] and is considerably greater than those of $(SO_2F)_2NXe^+$ (−1943 ppm, SbF_5 solvent, 25 °C)[5] and isoelectronic F_5TeOXe^+ (−1472 ppm, SbF_5 solvent, 5 °C).[33] The $^{129}Xe-^{14}N$ scalar coupling is not observed because of quadrupolar relaxation of ^{14}N resulting from the low symmetry at nitrogen in $F_5TeN(H)Xe^+$. The ^{129}Xe NMR spectrum of 99.5% ^{15}N-enriched $[F_5TeN(H)Xe][AsF_6]$ is a doublet centered at −2841 ppm in HF solvent at −45 °C, $^1J(^{129}Xe-^{15}N) = 138$ Hz (Figure 5b), and at −2902 ppm in BrF_5 solvent at −45 °C, $^1J(^{129}Xe-^{15}N) = 142$ Hz, compared with $^1J(^{129}Xe-^{15}N) = 91.7$ Hz in $(FO_2S)_2NXe^+$.[5] The broad line widths of the ^{129}Xe NMR spectra of $F_5Te^{15}N(H)Xe^+$ recorded at 11.7440 T in HF and BrF_5 solvents ($\Delta\nu_{1/2} \approx 80$ Hz) precluded the observation of the long-range couplings to xenon, namely,

(32) Gerken, M.; Schrobilgen, G. J. *Coord. Chem. Rev.* **2000**, *197*, 335.
(33) Keller, N.; Schrobilgen, G. J. *Inorg. Chem.* **1981**, *20*, 2118.

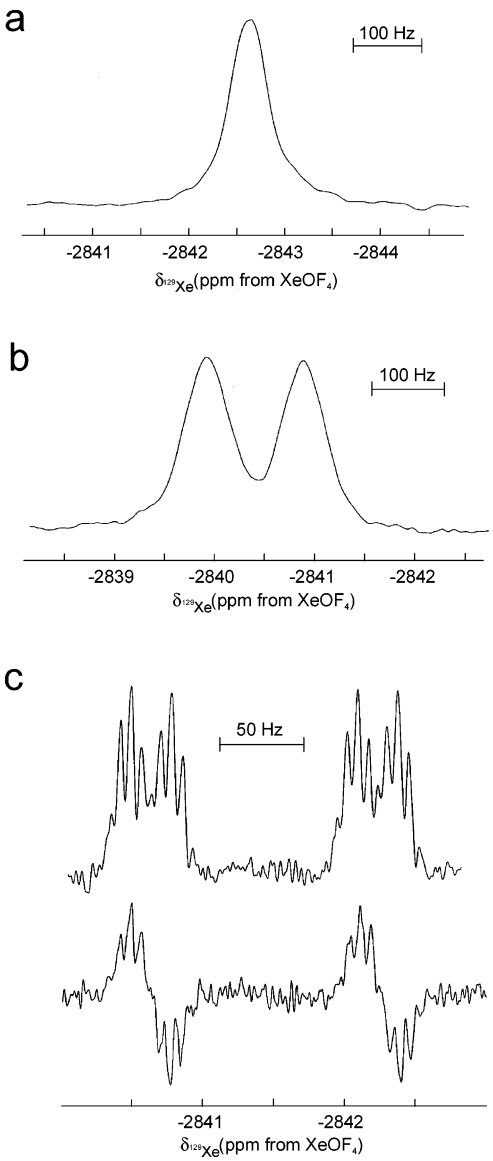

Figure 5. ^{129}Xe NMR spectra of $[F_5TeN(H)Xe][AsF_6]$ in HF solvent: (a) natural abundance sample recorded at −45 °C (139.051 MHz, 11.7440 T), (b) 99.5% ^{15}N-enriched sample recorded at −45 °C (139.051 MHz, 11.7440 T), and (c) (upper trace) 99.5% ^{15}N-enriched sample recorded at −39 °C (83.445 MHz, 7.0463 T) resolution enhanced by Gaussian multiplication and (lower trace) the $^{129}Xe-^1H$ INEPT spectrum which was also resolution enhanced by Gaussian multiplication.

$^2J(^{129}Xe-^1H)$, $^2J(^{129}Xe-^{125}Te)$, $^3J(^{129}Xe-^{19}F_a)$, and $^3J(^{129}Xe-^{19}F_e)$, which is, in large measure, attributable to the relaxation of ^{129}Xe by shielding anisotropy (SA). Relaxation by SA is proportional to the square of the external magnetic field, B_o, and is precedented by the field dependence of the ^{129}Xe line width of 30% ^{15}N-enriched $(FO_2S)_2NXe^+$ in SbF_5 solvent.[5] A substantial line width reduction for the ^{129}Xe resonance of $F_5TeN(H)Xe^+$ at $B_o = 7.0463$ T in HF solvent at −39 °C was obtained, confirming a significant SA contribution to the T_1 relaxation. Application of a Gaussian line-shape function to the free-induction decay of the 7.0463 T ^{129}Xe NMR spectrum prior to Fourier transformation (Figure 5c; upper trace) gave a doublet of doublets of quintets resulting from $^1J(^{129}Xe-^{15}N) = 136$ Hz and $^2J(^{129}Xe-^1H) = 24$ Hz and a quintet resulting from the coupling of four chemically

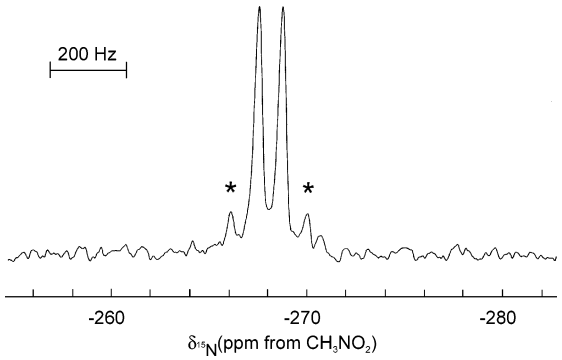

Figure 6. ^{15}N NMR spectrum (50.698 MHz) of 99.5% ^{15}N-enriched [F_5TeN(H)Xe][AsF_6] in HF solvent at −40 °C. Asterisks denote ^{129}Xe satellites resulting from $^1J(^{129}Xe-^{15}N)$; the inner peak of each satellite doublet overlaps with a peak of the central doublet.

equivalent equatorial fluorine atoms (F_e) bonded to tellurium ($^3J(^{129}Xe-^{19}F_e) = 6$ Hz). The magnitude of $^3J(^{129}Xe-^{19}F_e)$ is, however, significantly less than that observed in F_5TeOXe$^+$ (18.5 Hz),[33] F_5TeOXeF (30 Hz),[34] and Xe(OTeF_5)$_2$ (31 Hz).[34] The coupling to the axial fluorine, F_A, $^3J(^{129}Xe-^{19}F_A)$, was not resolved nor has this coupling been resolved in the ^{129}Xe NMR spectra of F_5TeOXe$^+$,[33] F_5TeOXeF,[34] and Xe(OTeF_5)$_2$.[34] The $^2J(^{129}Xe-^{125}Te)$ coupling was not observed in either the ^{129}Xe or ^{125}Te NMR spectra of F_5TeN(H)Xe$^+$ and XeOTeF_5^+,[33] but it was observed in those of F_5TeOXeF and Xe(OTeF_5)$_2$.[34] The assignment of the 24 Hz doublet splitting to $^2J(^{129}Xe-^1H)$ was confirmed by a ^{129}Xe−^{1}H INEPT experiment (Figure 5c; lower trace).

The ^{15}N NMR spectrum of [^{15}N]F_5TeN(H)Xe$^+$ in HF solvent at −40 °C (Figure 6), is a doublet centered at −268.0 ppm, $^1J(^{15}N-^1H) = 62$ Hz, and it is flanked by satellite doublets from $^1J(^{129}Xe-^{15}N) = 138$ Hz (natural abundance ^{129}Xe, 26.44%; $I = {}^1/_2$; the inner peaks of each satellite doublet are coincident with the central doublet peaks), in good agreement with the coupling observed in the ^{129}Xe NMR spectrum. The ^{15}N NMR parameters in BrF_5 solvent at −45 °C were −266.3 ppm and $^1J(^{15}N-^1H) = 62$ Hz; the satellite spectrum resulting from the $^1J(^{129}Xe-^{15}N)$ coupling was not observed in BrF_5 solvent because of the low signal-to-noise ratio. The ^{15}N chemical shift is similar to those reported for FXeN(SO_2F)$_2$ (−247.9 ppm; SO_2ClF, −40 °C),[4] Xe[N(SO_2F)$_2$]$_2$ (−232.5 ppm; SO_2ClF, −40 °C),[4] and XeN(SO_2F)$_2^+$ (−243.0 ppm; SbF_5, 25 °C).[5]

The ^{1}H NMR spectrum of natural abundance F_5TeN(H)Xe$^+$ in BrF_5 solvent (−56 °C) consisted of a singlet at 6.90 ppm; no coupling to ^{14}N was observed as a result of quadrupolar relaxation, but a satellite doublet resulting from $^2J(^{125}Te-^1H) = 46$ Hz was observed (Figure 7a). The proton−nitrogen coupling, $^1J(^{15}N-^1H) = 62$ Hz, was observed in the ^{1}H NMR spectrum of [^{15}N]F_5TeN(H)Xe$^+$ in BrF_5 solvent at −44 °C (Figure 7b). Failure to observe the $^2J(^{129}Xe-^1H)$ coupling (24 Hz) is attributed to broadening of the ^{129}Xe satellites resulting from an increased SA contribution to T_1 at the higher external field strength (B_o = 11.7440 T) used to obtain the ^{1}H NMR spectra and to the higher viscosity of BrF_5.

(34) Seppelt, K.; Rupp, H. H. *Z. Anorg. Allg. Chem.* **1974**, *409*, 338.

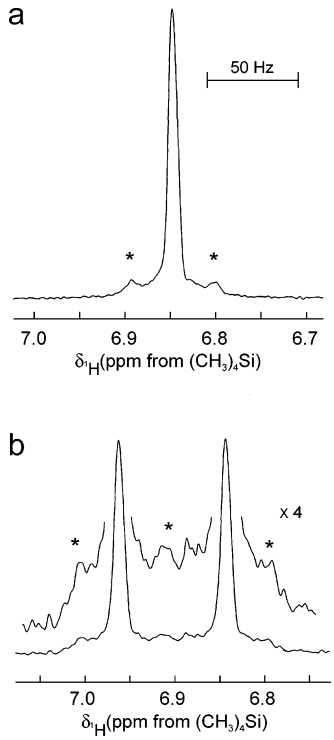

Figure 7. ^{1}H NMR spectra (500.138 MHz) of [F_5TeN(H)Xe][AsF_6] in BrF_5 solvent: (a) natural abundance sample recorded at −56 °C and (b) 99.5% ^{15}N-enriched sample recorded at −44 °C. Asterisks denote ^{125}Te satellites resulting from $^2J(^{125}Te-^1H)$.

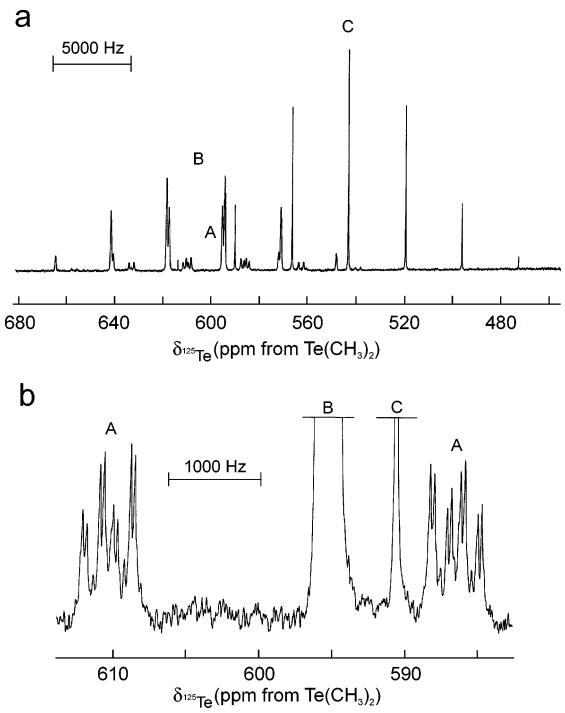

Figure 8. ^{125}Te NMR spectrum (157.795 MHz) resulting from the reaction of 99.5% ^{15}N-enriched [F_5TeNH_3][AsF_6] and XeF_2 in HF solvent (−34 °C): (a) multiplet center of (A) F_5TeN(H)Xe$^+$, (B) F_5TeNH_3^+, and (C) TeF_6 and (b) expansion of the central transitions of the F_5TeN(H)Xe$^+$ multiplet (A) showing the $^1J(^{125}Te-^{15}N)$ and $^2J(^{125}Te-^1H)$ couplings.

The ^{125}Te NMR spectrum of an equimolar mixture of [^{15}N]F_5TeNH_2 and [XeF][AsF_6] in HF solvent (−34 °C; Figure 8a) resulted in an equilibrium mixture of the F_5TeN(H)Xe$^+$ and F_5TeNH_3^+ cations (eq 9), with multiplets

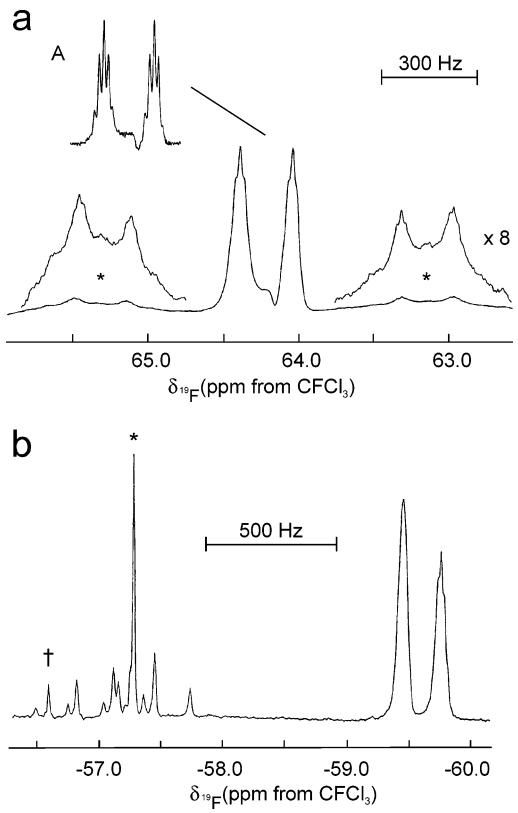

Figure 9. ^{19}F NMR spectrum (470.599 MHz) of 99.5% ^{15}N-enriched F_5TeNF_2 in BrF_5 solvent at −60 °C: (a) the F-on-N environment (F_N) (asterisks denote ^{125}Te satellites resulting from $^2J(^{125}Te-^{19}F_N) = 1025$ Hz), (A) the resolution of the central doublet of quintets enhanced by Gaussian multiplication of the free induction decay before Fourier transformation, and (b) the AB_4 spectrum of the F_5Te group (the asterisk and dagger denote the ^{125}Te and ^{123}Te satellites, respectively, that result from $^1J(^{125}Te-^{19}F)$ and $^1J(^{123}Te-^{19}F)$ of TeF_6 also present in the sample).

assigned to $F_5TeN(H)Xe^+$ (doublet of quintets, 598 ppm), $F_5TeNH_3^+$ (doublet of quintets, 607 ppm), and the decomposition product TeF_6 (septet, 543 ppm). The doublet of quintets ^{125}Te NMR spectrum of $F_5TeN(H)Xe^+$ resulting from $^1J(^{125}Te-^{19}F_a) = 3578$ Hz and $^1J(^{125}Te-^{19}F_e) = 3766$ Hz is further split into a doublet of doublets by coupling to ^{15}N and ^1H ($^1J(^{125}Te-^{15}N) = 333$ Hz and $^2J(^{125}Te-^1H) = 46$ Hz) (Figure 8b). The ^{125}Te chemical shift is comparable to that of the isoelectronic F_5TeOXe^+ cation (576 ppm; SbF_5 solvent, 25 °C).[33]

(d) F_5TeNF_2. The structure of F_5TeNF_2 was determined from the ^{19}F and ^{15}N NMR spectra of the natural abundance and 99.5% ^{15}N-enriched compounds in HF and BrF_5 solvents and is in agreement with Structure IV. The fluorine-on-nitrogen resonance of natural abundance F_5TeNF_2 (BrF_5 solvent, −60 °C) consists of a broad singlet at 64.2 ppm ($\Delta\nu_{1/2} = 209$ Hz) which results from the quadrupole collapse of the $^1J(^{19}F_N-^{14}N)$ coupling (^{14}N, $I = 1$) (Figure 9a). The chemical shift is similar to those of other difluoramine compounds (e.g., F_5SNF_2[35] (68.2 ppm) and F_2N-NF_2[36] (60.4 ppm)). The ^{19}F NMR spectrum of 99.5% ^{15}N-enriched F_5TeNF_2 (BrF_5 solvent, −44 °C) is a broad doublet centered

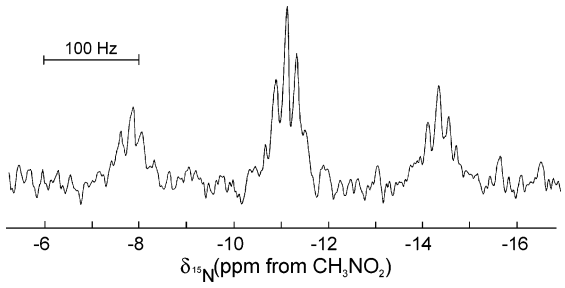

Figure 10. ^{15}N NMR spectrum (50.698 MHz) of 99.5% ^{15}N-enriched F_5TeNF_2 in BrF_5 solvent at −57 °C.

at 64.2 ppm (Figure 9b) resulting from $^1J(^{19}F-^{15}N) = 165$ Hz and is flanked by satellite doublets assigned to $^2J(^{125}Te-^{19}F_N) = 1025$ Hz. Gaussian multiplication resulted in resolution of the quintet structure resulting from $^3J(^{19}F_N-^{19}F_e) = 15$ Hz. The $^3J(^{19}F_N-^{19}F_a)$ coupling was not resolved, which is in accordance with the general inability to resolve three-bond couplings involving the axial fluorine of F_5Te derivatives (e.g., $^3J(^{129}Xe-^{19}F_a)$ in F_5TeOXe^+,[33] $Xe(OTeF_5)_2$,[34] $FXeOTeF_5$,[34] and $F_5TeN(H)Xe^+$).

The fluorine-on-tellurium(VI) region of the ^{19}F NMR spectrum ($B_o = 11.7440$ T) of 99.5% ^{15}N-enriched F_5TeNF_2 (BrF_5 solvent; −60 °C) consists of an AB_4 pattern (Figure 9b). The individual transitions of the B_4 portion of the spectrum were not resolved because of further splitting of each transition into a triplet of doublets by $^2J(^{19}F_e-^{15}N) = 11$ Hz (obtained from the ^{15}N NMR spectrum) and $^3J(^{19}F_N-^{19}F_e) = 15$ Hz. The ^{19}F chemical shifts of the axial and equatorial fluorine environments were −57.3 and −59.5 ppm, respectively, and $^2J(^{19}F_a-^{19}F_e)$ was 148 Hz.

The ^{15}N NMR spectrum of 99.5% ^{15}N-enriched F_5TeNF_2 in BrF_5 solvent at −57 °C (Figure 10) consists of a triplet of quintets centered at $\delta(^{15}N) = -11.1$ ppm. The quintet structure results from the coupling of ^{15}N with the four equatorial fluorines of the F_5Te group ($^2J(^{19}F_e-^{15}N) = 11$ Hz). The triplet splitting results from $^1J(^{19}F-^{15}N)$ (165 Hz), confirming the coupling observed in the ^{19}F NMR spectrum (Figure 9b). It is noteworthy that the ^{15}N chemical shifts of NF_3 ($\delta(^{15}N) = -14$ ppm)[37] and F_5TeNF_2 are similar and are consistent with the high electronegativity of the F_5Te group.

The ^{125}Te resonance of F_5TeNF_2 was not observed because of the low concentration of F_5TeNF_2.

Computational Results. Electronic structure calculations at the local density functional theory (LDFT) and Hartree−Fock (HF) levels were done for $F_5TeN(H)Xe^+$, the $[F_5TeN(H)Xe][AsF_6]$ ion pair, F_5TeNH_2, $F_5TeNH_3^+$, and F_5TeNF_2 to support the vibrational assignments and to gain more insight into the structures and bonding of these molecules. Calculations at the gradient-corrected (B3LYP) and MP2 levels were also done for $F_5TeN(H)Xe^+$ and the $[F_5TeN(H)Xe][AsF_6]$ ion pair (Table S2). The $^{14}N/^{15}N$ isotope shifts for the vibrational frequencies were calculated at the HF level. The Te−F bond length and vibrational frequencies of TeF_6 were calculated for use as benchmarks (see Supporting Information). The DFT calculations provided the best agreement and reproduced the trends among the F_5Te derivatives considered at all levels. The electronic structure of the

(35) Stump, Jr., E. C.; Padgett, C. D.; Brey, W. S., Jr. *Inorg. Chem.* **1963**, *2*, 648.
(36) Colburn, C. B.; Johnson, F. A.; Haney, C. *J. Chem. Phys.* **1965**, *43*, 4526.

Table 4. NPA Charges,[a] Mulliken Charges,[b] Mayer Valencies,[b] and Mayer Bond Orders[b] for $F_5TeNH_3^+$, $F_5TeN(H)Xe^+$, F_5TeNF_2, F_5TeNH_2, and F_5TeN^{2-}[c]

charges and valencies[d]

	$F_5TeNH_3^+$			$F_5TeN(H)Xe^+$			F_5TeNF_2			F_5TeNH_2			F_5TeN^{2-}		
atom	NPA	Mul	val	NPA	Mul	val	NPA	Mul	val	NPA	Mul	val	NPA	Mul	val
Te	3.42	1.22	6.30	3.41	1.21	6.31	3.26	1.23	6.08	3.39	1.18	6.32	2.91	1.16	5.90
F_a	−0.53	−0.18	1.21	−0.54	−0.19	1.19	−0.57	−0.25	1.08	−0.58	−0.26	1.07	−0.66	−0.43	1.21
F_e	−0.56	−0.21	1.16	−0.57	−0.22	1.11	−0.58	−0.25	1.11	−0.60	−0.28	1.06	−0.69	−0.47	1.16
N	−1.21	−0.33	3.41	−1.14	−0.16	2.85	0.04	0.16	2.91	−1.32	−0.40	3.05	−1.48	−0.83	3.41
Xe				1.04	0.66	1.19									
H	0.52	0.37	0.87	0.50	0.36	0.85				0.46	0.29	0.92			
F							−0.20	−0.06	1.10						

bond orders[d]

bond	$F_5TeNH_3^+$	$F_5TeN(H)Xe^+$	F_5TeNF_2	F_5TeNH_2	F_5TeN^{2-}
Te−F_a	1.13	1.12	1.03	1.02	0.77
Te−F_e	1.08	1.06	1.03	1.01	0.67
Te−N	0.81	0.90	0.84	1.22	2.45
N−Xe		1.06			
N−H	0.84 H 3	0.82		0.89 H 2	
N−F			0.97 H 2		

[a] DZVP basis set. [b] DZVP2 basis set. [c] Labels correspond to those used in Structures I (F_5TeNH_2), II ($F_5TeNH_3^+$), III ($F_5TeN(H)Xe^+$), and IV (F_5TeNF_2). [d] Average values are reported for F_e where they are not symmetry equivalent.

unknown F_5TeN^{2-} anion, which is isoelectronic with the F_5TeO^- anion, was calculated for comparison (Tables 2, 4, and S3). The calculated geometrical parameters of $F_5TeN(H)Xe^+$, F_5TeNH_2, $F_5TeNH_3^+$, F_5TeNF_2, and F_5TeN^{2-} are listed and compared in Table 2 and are discussed in the Supporting Information.

(a) Charges, Valencies, and Bond Orders. The natural population analysis (NPA) charges, Mayer valencies, and bond orders[38−41] are given in Table 4. The latter properties have been used instead of Mulliken overlaps because the Mayer values provide more reasonable values and insights into the bonding and are not strongly basis set dependent.[28,42,43] The valencies for Te in $F_5TeN(H)Xe^+$, F_5TeNH_2, $F_5TeNH_3^+$, and F_5TeNF_2 range from 6.08 to 6.32 as expected for six coordination. The lower valency value for F_5TeNF_2 (6.08) is consistent with the very long Te−N bond. The valencies of the F atoms range from 1.04 to 1.21, with the largest values for F_a, which is always the shortest Te−F bond except for F_5TeNF_2. The Te−F bond orders range from 0.98 to 1.13 for the various derivatives, showing essentially single Te−F bonds. The Te−N bond orders show a significant variation with Te substituent: 0.81 (NH_3^+), 0.84 (NF_2), 0.90 ($N(H)Xe^+$), and 1.22 (NH_2). Interestingly, addition of a proton to F_5TeNH_2 leads to a significant reduction in the Te−N bond order to 0.81, consistent with the large increase in the Te−N bond length and increases in the Te−F bond orders. This demonstrates the usefulness of Mayer properties. The charge on the Te atom is very similar over the series. The Te atom valency in F_5TeN^{2-} is only 5.90, and the N atom valency is 3.41. As expected, the N atom has a greater negative charge in the dianion, −1.48/−0.83 (NPA/Mulliken), compared with the charge of −1.32/−0.40 in F_5TeNH_2, with most of the negative charge localized on the fluorine atoms of the dianion.

Most of the positive charge on $F_5TeN(H)Xe^+$ is localized on the Xe (1.04/0.66) and H (0.50/0.36) atoms. The N valency is 2.85, which is consistent with sp^3 hybridization at the N atom. The Xe atom has a valency of 1.19, suggesting a strong bonding interaction with nitrogen. The Xe−N bond order is 1.06, which is consistent with a single covalent bond between nitrogen and xenon. The Te−N bond order of 0.90 shows no evidence of an increased covalent (π-bonding) interaction with the Te atom, consistent with trigonal pyramidal coordination at the N atom.

(b) Natural Bond Orbital (NBO) Analyses. The NBO analyses[44,45] have been performed using a polarized double-ζ basis set[46−51] at the DFT level (Table S4). The NBO analyses predict the Te atoms to have more positive charge and the F

(37) Qureshi, A. M.; Ripmeester, J. A.; Aubke, F. *Can. J. Chem.* **1969**, *47*, 4247.
(38) Mayer, I. *Chem. Phys. Lett.* **1983**, *97*, 270.
(39) Mayer, I. *Theor. Chim. Acta* **1985**, *67*, 315.
(40) Mayer, I. *Int. J. Quantum Chem.* **1986**, *29*, 73.
(41) Mayer, I. *Int. J. Quantum Chem.* **1986**, *29*, 477.
(42) Fir, B. A.; Mercier, H. P. A.; Sanders, J. C. P.; Dixon, D. A.; Schrobilgen, G. J. *J. Fluorine Chem.* **2001**, *110*, 89.
(43) Casteel, W. J., Jr.; Dixon, D. A.; Mercier, H. P. A.; Schrobilgen, G. J. *Inorg. Chem.* **1996**, *35*, 4310.
(44) Hay, P. J.; Wadt, W. R. *J. Chem. Phys.* **1985**, *82*, 270, 284, 299.
(45) Frisch, M. J.; Trucks, G. W.; Schlegel, H. B.; Scuseria, G. E.; Robb, M. A.; Cheeseman, J. R.; Zakrzewski, V. G.; Montgomery, J. A., Jr.; Stratmann, R. E.; Burant, J. C.; Dapprich, S.; Millam, J. M.; Daniels, A. D.; Kudin, K. N.; Strain, M. C.; Farkas, O.; Tomasi, J.; Barone, V.; Cossi, M.; Cammi, R.; Mennucci, B.; Pomelli, C.; Adamo, C.; Clifford, S.; Ochterski, J.; Petersson, G. A.; Ayala, P. Y.; Cui, Q.; Morokuma, K.; Malick, D. K.; Rabuck, A. D.; Raghavachari, K.; Foresman, J. B.; Cioslowski, J.; Ortiz, J. V.; Stefanov, B. B.; Liu, G.; Liashenko, A.; Piskorz, P.; Komaromi, I.; Gomperts, R.; Martin, R. L.; Fox, D. J.; Keith, T.; Al-Laham, M. A.; Peng, C. Y.; Nanayakkara, A.; Gonzalez, C.; Challacombe, M.; Gill, P. M. W.; Johnson, B. G.; Chen, W.; Wong, M. W.; Andres, J. L.; Head-Gordon, M.; Replogle, E. S.; Pople, J. A. *Gaussian 98*, revision A.7; Gaussian, Inc.: Pittsburgh, PA, 1998.
(46) Dunning, T. H., Jr.; Hay, P. J. In *Methods of Electronic Structure Theory*; Schaefer, H. F., III, Ed.; Plenum Press: New York, 1977; p 1.
(47) Reed, A. E.; Curtiss, L. A.; Weinhold, F. *Chem. Rev.* **1988**, *88*, 899.
(48) Foster, J. P.; Weinhold, F. *J. Am. Chem. Soc.* **1980**, *102*, 7211.
(49) Reed, A. E.; Weinhold, F. *J. Chem. Phys.* **1983**, *78*, 4066.
(50) Reed, A. E.; Weinstock, R. B.; Weinhold, F. *J. Chem. Phys.* **1985**, *83*, 735.
(51) Reed, A. E.; Weinhold, F. *J. Chem. Phys.* **1985**, *83*, 1736.

atoms to have more negative charge than the Mulliken values. Thus, the NPA values show larger degrees of charge separation, corresponding to more ionic bond character than do the Mulliken charges, but both are consistent with significantly ionic structures. The NBO analyses show that the Te−F bonds are highly ionic with 85−88% of the nominal two electrons in the bond being on the F atom (Table S4). The electrons on the F atom are found to be in orbitals having high p character. The Te component (12−15% or 0.24−0.30 e) has mainly sp^3 hybridization with some d orbital participation. There are 1.85−1.90 e in the σ(Te−F) orbitals and 0.18−0.20 e in the σ(Te−F)* orbitals. The Te−N bond in $F_5TeN(H)Xe^+$ is similar to the Te−F bonds except that there is a slightly higher Te component. The Xe−N bond is almost equally shared between N and Xe and is almost pure p in character with 1.99 e in the σ(Xe−N) orbital and only 0.05 e in the σ(Xe−N)* orbital. The Te−N bonds in F_5TeNH_2, $F_5TeNH_3^+$, and $F_5TeN(H)Xe^+$ are similar. The Te−N bond in F_5TeNF_2 has a much higher p character on the N atom and less population in the s component, in accord with the very long Te−N bond (Table 2). The NBO structure for F_5TeN^{2-} differs in that the anion is predicted to have three Te−N bonding contributions. The first bonding contribution is predicted to be 34% Te character (0.62 e). The remaining two bonding contributions are somewhat delocalized N 2p orbital lone pairs, each having 12% Te character (0.23 e). Thus, the Te−N bond is best described by an ionic σ(Te−N) bond with additional stabilization from back-donation of two N lone pairs to the Te atom. As noted in the above discussion, the bonds to Te in the hexacoordinate species are highly ionic, consistent with most of the population in each bond localized on the ligand and not on the Te atom. However, the NBO analysis does show 6 bonds to Te (except for F_5TeN^{2-} as discussed above) consistent with a Mayer valency of near 6 for Te. The importance of ionic bonding in these systems is consistent with the postulates of Reed and Schleyer,[52] who suggested that the bonding in F_5TeN^{2-} and F_5TeNH_2 is predominantly ionic, and with the present NBO results. The stability of F_5TeN^{2-} comes from the back-bonding of the lone pairs on N to the Te, in accordance with the acidity of F_5TeNH_2.[14,53]

The valence s orbital populations on the N atom bonded to Te show some interesting variations with the largest s population on the N atom of $F_5TeN(H)Xe^+$ followed by the F_5TeNH_2: 1.69 e ($F_5TeN(H)Xe^+$), 1.59 e (F_5TeNH_2), 1.55 e (F_5TeNF_2), and 1.53 e ($F_5TeNH_3^+$). The two species with the longest Te−N bonds have the lowest s orbital characters. The valence s orbital populations on the Te are as follows: 0.94 e ($F_5TeN(H)Xe^+$), 1.06 e (F_5TeNF_2), 0.94 e (F_5TeNH_2), and 0.94 e ($F_5TeNH_3^+$). The only exception is the NF_2 derivative which has a very long Te−N bond of very high p character. The magnitudes of the $^1J(^{125}Te-^{15}N)$ couplings for $F_5TeN(H)Xe^+$ (333 Hz) and F_5TeNH_2 (231 Hz), which are large when compared with that of $F_5TeNH_3^+$ (48 Hz), correlate with the s populations on their respective N atoms and with the Te and N s electron contributions to the Te−N

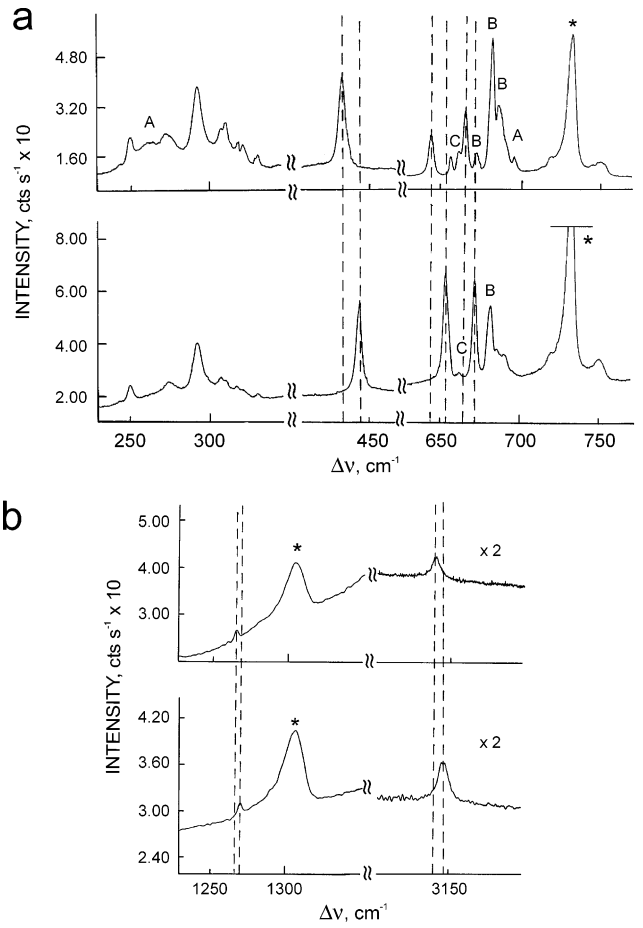

Figure 11. Raman spectra of natural abundance (lower trace) and 99.5% ^{15}N-enriched (upper trace) $[F_5TeN(H)Xe][AsF_6]$ recorded at −165 °C using 514.5 nm excitation: (a) 200−800 cm^{-1} region and (b) 1200−1350 and 3100−3200 cm^{-1} regions. The labels denote (A) $[Xe_2F_3][AsF_6]$, (B) $[F_5TeNH_3][AsF_6]$, and (*) the FEP sample tube lines.

σ bonds (i.e., s Te 15.7%, s N 21.1% ($F_5TeN(H)Xe^+$); s Te 21.1%, s N 21.4% (F_5TeNH_2); and s Te 13.9%, s N 18.4% ($F_5TeNH_3^+$)), and appear to be consistent with a significant Fermi contact contribution to the coupling.[54] These coupling constants also correlate with the experimental and calculated Te−N bond lengths, with $F_5TeN(H)Xe^+$ and F_5TeNH_2 exhibiting the shortest Te−N bonds and largest $^1J(^{125}Te-^{15}N)$ couplings.

Raman Spectroscopy. The solid-state Raman spectra of natural abundance and 99.5% ^{15}N-enriched $[F_5TeN(H)Xe][AsF_6]$, F_5TeNH_2, and $[F_5TeNH_3][AsF_6]$ are shown in Figures 11 and S5−S7, respectively. The $[F_5TeN(H)Xe][AsF_6]$ spectra were obtained from mixtures of $[Xe_2F_3][AsF_6]$, $[F_5TeNH_3][AsF_6]$, and $[F_5TeN(H)Xe][AsF_6]$ whose relative amounts varied from sample to sample, preventing a rigorous assignment of the anion bands for $[F_5TeN(H)Xe][AsF_6]$ (see Supporting Information). The observed and calculated frequencies and their assignments are listed in Tables 5−7 and

(52) Reed, A. E.; Ragué-Schleyer, P. *J. Am. Chem. Soc.* **1990**, *112*, 1434.
(53) Klöter, G.; Seppelt K. *J. Am. Chem. Soc.* **1979**, *101*, 347.
(54) Sanders, J. C. P.; Schrobilgen, G. J In *A Methodological Approach to Multinuclear NMR in Liquids and Solids-Chemical Applications*; Granger, P., Harris, R. K., Eds.; NATO Advanced Study Institute, Magnetic Resonance; Kluwer Academic Publishers: Dordrecht, The Netherlands, 1990; Chapter 11, pp 157−186.
(55) Pople, J. A.; Scott, A. P.; Wong, M. W.; Radom, L. *Isr. J. Chem.* **1993**, *33*, 345.

Table 5. Raman Frequencies for F_5TeNH_2 and Calculated Vibrational Frequencies, Assignments, and Mode Descriptions for F_5TeNH_2 and F_5TeNF_2

frequencies (cm^{-1})									
α-F_5TeNH_2 (expt)l			F_5TeNH_2 (calcd)			F_5TeNF_2 (calcd)			
^{14}N[a]	^{15}N[a]	$\Delta\nu(^{15}N-^{14}N)$	DFT[b]	HF[b,c]	$\Delta\nu(^{15}N-^{14}N)$[d]	DFT[b]	HF[b,c]	$\Delta\nu(^{15}N-^{14}N)$[d]	assignments (C_1)[e]
3385.3 (17)	3376.1 (13)	−9.2	3568 (88)	3502 (100)	−11.8				$\nu_{as}(NH_2)$
3297.2 (76)	3292.9 (57)	−4.3	3487 (71)	3392 (66)	−5.2				$\nu_{sym}(NH_2)$
3280.1 sh	3275.8 (3)	−4.3							
1514.2 br	1509.3 (1)	−4.9	1493 (58)	1534 (48)	−4.8				$\delta(NH_2)$
						1037 (107)	1109 (63)	−26.2	$\nu_{sym}(NF_2)$
1028.4 (2)	1024.8 (1)	−3.6	985 (18)	987 (27)	-4.7				NH_2 rock
						923 (176)	1070 (119)	−24.8	$\nu_{as}(NF_2)$
761.0 (10)	752.9 (6)	−8.1	746 (58)	712 (95)	-8.6				NH_2 inversion + ν(Te−N)
						693 (114)	697 (128)	−0.3	ν(TeF6 − TeF2 + TeF5)
719.3 (2)	717.6 (1)	−1.7	697 (132)	681 (177)	0.0	687 (102)	697 (127)	−0.2	ν(TeF3 − TeF4)
			695 (163)	680 (166)	−0.5				ν(TeF5 − TeF6)
						687 (95)	690 (103)	−0.3	ν(TeF5)
689.1 (71)	688.5 (69)	−0.6							
680.4 (44)	681.0 (40)	0.6	662 (64)	660 (60)	−3.5				ν_{sym}(TeF) + ν(TeN) + NH_2 inversion
673.1 sh	673.4 sh	0.3							
628.6 sh	628.0 sh	-0.6	621 (2)	609 (0)	−1.8				ν(TeF5 + TeN) − ν(TeF3 + TeF4)
619.6 (84)	619.4 (76)	-0.2	609 (4)	602 (1)	-0.6				ν(TeF2 + TeF6) − smaller ν(TeF5+ TeN + TeF2 + TeF3)
						617 (2)	628 (1)	−0.1	ν(TeF3 + TeF4)
						615 (10)	620 (0)	−0.2	ν(TeF6 + TeF2)
						569 (19)	604 (3)	−14.3	ν(TeN) + FNF inversion
582.7 (100)	572.9 (100)	−9.8	544 (128)	537 (185)	−9.6				ν(TeN) + NH_2 inversion
						538 (0)	550 (2)	−8.2	δ(F−N−F)
			348 (39)	339 (33)	−0.1				δ(F6TeF5 + F3TeF4)
			337 (42)	334 (125)	−0.3				δ(F2TeF5 + F3TeF4)
						314 (57)	331 (49)	−0.7	δ(F3TeF4 + F2TeF6) o.o.p.
						314 (22)	329 (132)	0.0	δ(F2TeF6 + F5TeN) o.o.p.
336.8 (23)	336.6 (18)	−0.2	310 (30)	321 (51)	0.0				δ(F6TeF4 − F6TeF3) + δ(F5TeF4 − F4TeN)
326.8 (21)	326.5 (18)	−0.3	310 (31)	304 (1)	−0.2	311 (24)	319 (57)	0.0	δ(F3TeF4 + F5TeN) o.o.p.
300.7 (34)	298.8 (28)	−1.9	294 (0)	296 (24)	−2.7	284 (1)	303 (2)	−0.2	δ(F3TeF2 + F6TeF4) i.p. scissors
286.7 (24)	283.1 (23)	−3.6	282 (6)	284 (13)	−3.3				δ(F3TeN − F4TeN) + δ(F2TeF4 − F2TeF3)
278.9 sh	276.6 sh	−2.3							
						279 (1)	301 (0)	−1.2	δ(F3TeF5 − F4TeN) scissor
						249 (6)	279 (11)	−0.9	ν(TeN) + TeF bends
						224 (5)	237 (9)	0.0	δ(F3TeF4)
						221 (6)	234 (13)	−0.1	δ(F2TeF6)
			210 (0)	206 (0)	0.0	183 (0)	192 (0)	0.0	δ(F2TeF6 − F3TeF4)
210.4 (2)	210.0 (1)	−0.4	195 (4)	199 (4)	−1.5				δ(F5TeN − F3TeF4)
197.3 br	194.6 br	−2.7	167 (1)	182 (26)	−1.1				δ(F5TeN − F6TeF2)
						133 (0)	149 (0)	−0.1	F_5Te group i.p. rock = (NF2)TeF5 bend
						124 (1)	133 (2)	−0.1	F_5Te group o.o.p. rock = (NF2)TeF5 bend
67.5 (2)	67.5 (3)	0.0	64 (25)	150 (7)	−0.2				NH_2 torsion
						30 (0)[f]	8 (0)	0.0	Te−N torsion
91.0 (1)	91.8 (2)	0.8							lattice modes
41.2 (8)	42.0 (4)	0.8							

[a] Values in parentheses denote relative Raman intensities. Abbreviations denote a shoulder (sh) and broad (br). [b] Infrared intensities (km mol^{-1}) are given in parentheses. [c] HF frequencies were scaled using a factor of 0.8953 according to ref 55. [d] Isotopic shifts were calculated at the HF level. [e] Abbreviations denote out-of-plane (o.o.p.) and in-plane (i.p.). [f] Estimated from an imaginary frequency.

Table 6. Raman Frequencies for $[F_5TeNH_3][AsF_6]$ and Calculated Vibrational Frequencies, Assignments, and Mode Descriptions for $F_5TeNH_3^+$

frequencies (cm^{-1})						assignments	
$[F_5TeNH_3][AsF_6]$ (exptl)			$F_5TeNH_3^+$ (calcd)			$F_5TeNH_3^+$ (C_1)	AsF_6^- (O_h)
^{14}N[a]	^{15}N[a]	$\Delta\nu(^{15}N-^{14}N)$	DFT[b]	HF [b,c]	$\Delta\nu(^{15}N-^{14}N)$[d]		
3110.1 br	3110.0 br	−0.1	3388 (190)	3325 (211)	−10.6	$\nu_{as}(NH_3)$	
			3383 (189)	3324 (210)	−10.7	$\nu_{as}(NH_3)$	
3018.0 br	3017.8 br	−0.2	3279 (129)	3219 (128)	−2.8	$\nu_{sym}(NH_3)$	
1539.7 br	1531.6 br	−8.1	1562 (50)	1573 (56)	−2.5	$\delta_{as}(NH_3)$	
			1551 (51)	1566 (56)	−2.4	$\delta_{as}(NH_3)$	
1405.7 (1)	1399.8 (<1)	−5.9	1360 (201)	1414 (210)	−8.6	$\delta_{sym}(NH_3)$ inv	
1396.9 (<1)	1391.2 (<1)	−5.7					
			888 (59)	887 (71)	−5.3	NH_3 rock	
			887 (59)	886 (70)	−5.3	NH_3 rock	
			736 (61)	730 (75)	−0.1	ν(TeF5)	
757.5 sh	756.1 sh	−1.4	735 (78)	723 (108)	−0.1	ν(TeF2 − TeF6)	
752.4 (4)	751.6 (3)	−0.8	734 (82)	723 (108)	−0.1	ν(TeF3 − TeF4)	
742.8 (3)	742.6 (3)	−0.2					
739.0 (2)							$\nu_3(T_{1u})$
730.3 (14)	729.3 (13)	−1.0					
716.0 (2)	714.7 (1)	−1.3					
688.8 sh	689.1 sh	0.3	666 (0)	654 (0)	−0.2	ν(TeF3 + TeF4) + ν(TeF2 + TeF6)	$\nu_1(A_{1g})$
682.9 (100)	682.2 (100)	−0.7					
671.6 (24)	671.5 (22)	−0.1	653 (0)	642 (0)	0.0	ν(TeF3 + TeF4) − ν(TeF6 + TeF2)	
592.9 (3)	589.0 sh	−3.9					
585.0 (10)	583.3 (9)	−1.7					$\nu_2(E_g)$
556.9 (8)							
548.1 (6)							
566.5 (18)	550.8 (18)	−15.7	502 (0)	466 (1)	−13.0	ν(Te−N)	
407.0 (1)	405.6 (1)	−1.4					$\nu_4(T_{1u})$
396.1 (<1)	395.4 (1)	−0.7					
376.8 (7)	376.1 (6)	−0.7					$\nu_5(T_{2g})$
373.1 (6)							
369.3 (7)	370.0 (6)	0.7	345 (56)	314 (144)	−0.1	δ(F2, F3, F4, F6) o.o.p.	
362.6 (3)	362.0 (3)	−0.6	332 (0)	313 (0)	0.0	δ(F2TeF3 + F4TeF6)	
355.5 (2)	354.7 (2)	−0.8	326 (30)	304 (53)	0.0	δ(F2TeF6 + F5TeN)	
			323 (33)	304 (54)	0.0	δ(F3TeF4 + F5TeN)	
321.1 (8)	320.4 (6)	−0.7	285 (2)	261 (1)	−1.4	δ(F3TeN − F6TeF2)	
315.7 (6)			271 (3)	260 (1)	−1.3	δ(F4TeN + F2TeF6)	
311.1 (20)	310.2 (17)	−0.9					
276.3 (6)	272.9 (5)	−3.4	218 (6)	188 (9)	−2.0	δ(F5TeN)	
			210 (7)	186 (9)	−2.0	δ(F5TeN) + TeF_5 rock	
			193 (2)	182 (0)	-0.1	δ(F2TeF6 − F3TeF4)	
203.1 br	201.4 br	−1.7	159 (4)	179 (0)	0.0	NH_3 torsion	

[a] Values in parentheses denote relative Raman intensities. Abbreviations denote a shoulder (sh) and broad (br). [b] Infrared intensities (km mol^{-1}) are given in parentheses. [c] HF frequencies were scaled using a factor of 0.8953 according to ref 55. [d] Isotopic shifts were calculated at the HF level.

S5. The spectral assignments were made by comparison with the frequencies obtained from density functional theory (DFT) and Hartree−Fock (HF) calculations. Assignments of modes involving the nitrogen atom were also supported by experimental and calculated $^{14}N/^{15}N$ isotopic shifts. In the case of the $F_5TeN(H)Xe^+$ cation, the frequency assignments were also compared with those of the isoelectronic F_5TeOXe^+ cation, whose assignments are based on frequencies derived from DFT calculations.[42] The modes of the distorted fluorine-bridged AsF_6^- anion were assigned by comparison with those of the $[F_5TeOXe][AsF_6]$ salt,[42] other xenon salts,[5,10,33] and KrF^+ salts.[28]

(a) α-F_5TeNH_2 and α-[^{15}N]F_5TeNH_2. Although F_5TeNH_2 was previously characterized by infrared and Raman spectroscopy in CH_2Cl_2 solution,[14] a fuller assignment of the vibrational bands of the low-temperature phase of F_5TeNH_2 is provided in Table 5.

The 21 vibrational modes of F_5TeNH_2 under C_s point symmetry belong to the irreducible representations 13A′ + 8A″, which are both Raman and infrared active. Using the unit cell from the −113 °C structure of α-F_5TeNH_2, a factor−group analysis (Table S6) was performed in which the free molecule symmetry (C_s) was correlated to the crystal site symmetry (C_1) and to the unit cell symmetry (C_2), leading to the prediction that each Raman- and infrared-active vibrational band of α-F_5TeNH_2 should be split into two Raman- and infrared-active components, A + B. Factor−group splittings were only resolved for three modes (Table 5).

The ensuing vibrational analysis of the F_5Te group presented in this section is also generally applicable to $F_5TeNH_3^+$ and $F_5TeN(H)Xe^+$, except where noted, and will not be discussed in detail for the cations. There is good overall agreement between the experimental and calculated DFT and scaled HF values (Table 5). The NH stretches occur at higher frequencies than those in $F_5TeNH_3^+$ and $F_5TeN(H)Xe^+$ (Tables 5−7). The rocking mode $\rho_r(NH_2)$ was observed as a weak band at 1028 cm^{-1} which displayed a $^{14}N/^{15}N$ isotopic shift (−3.6 cm^{-1}) in good agreement with the calculated value (−4.7 cm^{-1}). The highest Te−F stretching frequency, 719 cm^{-1}, appears at lower frequency than the T_{1u} mode of TeF_6 (751 cm^{-1}) from which it derives. The factor−group split Te−F stretch around 680 cm^{-1} is derived

Table 7. Experimental Raman Vibrational Frequencies for $[F_5TeN(H)Xe][AsF_6]$ and Calculated Vibrational Frequencies, Assignments, and Mode Descriptions for $F_5TeN(H)Xe^+$

frequencies (cm^{-1})						assignments	
$[F_5TeN(H)Xe][AsF_6]$ (expt)			$F_5TeN(H)Xe^+$ (calcd)			$F_5TeN(H)Xe^+$ (C_1)	AsF_6^- (O_h)
^{14}N[a]	^{15}N[a]	$\Delta\nu(^{15}N-^{14}N)$	DFT[b]	HF[b,c]	$\Delta\nu(^{15}N-^{14}N)$[d]		
3145.9 br	3138.8 br	−7.1	3322 (152)	3336 (167)	−8.6	ν(NH)	
1270.8 br	1268.3 br	−2.5	1224 (17)	1257 (2)	−3.1	δ(HNTe)	
			757 (80)	720 (112)	−0.5	NH inversion	
750.1 (19)	751.0 (22)	0.9	730 (77)	718 (129)	−0.7	ν(TeF5) + ν(TeF2 − TeF6)	
	745.6 sh		725 (72)	711 (119)	−0.1	ν(TeF5) + ν(TeF2 − TeF6)	
			716 (75)	689 (60)	−5.6	ν(TeF5) + ν(TeF4 − TeF3)	
720.4 (25)	719.9 (26)	−0.5					$\nu_3(T_{2g})$
	713.4 (8)						
690.8 (20)	696.9 (21)	6.1	653 (5)	651 (1)	−3.7	ν(TeF2 + TeF3 + TeF4 + TeF6)	
686.6 (25)	688.0 (92)	1.4					$\nu_1(A_{1g})$
672.3 (90)	666.1 (100)	−6.2	636 (3)	630 (2)	−0.1	ν(TeF2 + TeF6) − ν(TeF3 + TeF4)	
662.5 (4)	656.9(25)	−5.6					
654.1 (100)	644.6 (67)	−9.5	623 (5)	606 (7)	−15.8	ν(TeN − XeN)	
601.7 sh	603.7 sh	2.0					
573.7 (84)	574.6 sh	1.1					$\nu_2(E_g)$
570.4 (79)	571.5 sh	1.4					
543.2 br	548.1 (18)	4.8					
444.1 (86)	433.2 (76)	−10.9	432 (37)	385 (3)	−11.5	ν(TeN + XeN)	
401.5 (11)	401.2 (15)	−0.3					$\nu_4(T_{1u})$
397.3(4)							
379.4 (36)	380.0 (60)	0.6					$\nu_5(T_{2g})$
375.8 (26)	376.0 sh	0.2					
			345 (90)	315 (51)	0.0	δ(F3TeF4 + F2TeF6) o.o.p. bend	
369.9 (15)			342 (27)	312 (184)	−0.3	δ(F3TeF4) + (F5TeF2 − F5TeF6)	
366.5 (20)	368.5 (36)	2.0	330 (15)	308 (45)	−0.2	δ(F2TeF4 + F3TeF6 + F5TeN)	
363.2 (10)			322 (15)	306 (43)	−0.2	δ(F2TeF3 + F4TeF6 + F5TeN)	
329.8 (5)	330.1 (9)	0.3					
320.0 (10)	321.1 (20)	1.1	292 (2)	264 (16)	−1.4	δ(F3TeF4)	
316.7 (13)	317.8 (22)	1.1					
306.9 (22)	307.4 (34)	0.5	255 (3)	239 (11)	−0.5	δ(F2TeF6)	
274.4 (21)	273.3 (32)	−1.1					
250.3 (19)	250.9 (22)	0.6	217 (2)	196 (2)	−0.3	δ(F5TeN)	
243.3 (10)	244.2 (7)	0.9	207 (2)	170 (3)	−1.4	δ(F3TeF4 − F3TeF4)	
201.6 (6)	202.7 (5)	1.1	160 (1)	147 (1)	0.0	δ(F5TeN)	
186.5 (3)	186.2 (3)	−0.3					
170.0 sh	169.1 sh	−0.9					
159.3 sh	159.6 sh	0.3					
113.4 (7)	114.2 (12)	0.8	100 (2)	93 (1)	−0.3	δ(XeNTe)	
105.0 (3)	105.3 (4)	0.3					
90 br	90 (br)	0.0	41 (1)	37 (1)	−0.3	torsion about TeN	
75 br	75 (br)	0.0					

[a] Values in parentheses denote relative Raman intensities. Abbreviations denote a shoulder (sh) and broad (br). [b] Infrared intensities (km mol^{-1}) are given in parentheses. [c] HF frequencies were scaled using a factor of 0.8953 according to ref 55. [d] Isotopic shifts were calculated at the HF level.

from the A_{1g} mode of TeF_6 (697 cm^{-1}) and shows a small frequency shift relative to it, whereas the Te−F stretches derived from the E_g mode of TeF_6 (670 cm^{-1}) also appear at lower frequencies (620 and 629 cm^{-1}). The antisymmetric and symmetric stretches are higher and lower, respectively, than those of $F_5TeNH_3^+$ and $F_5TeN(H)Xe^+$ (Tables 6 and 7). The inversion of the NH_2 group is coupled to the Te−N stretch with the high-frequency component at 761 cm^{-1}. The low-frequency, factor−group split component is at 673 (shoulder), 680, and 689 cm^{-1} and shows a significant Te−F stretching contribution. The higher component has a $^{14}N/^{15}N$ isotope shift of −8.1 cm^{-1} (calcd, −8.6 cm^{-1}). The Te−N stretch is coupled to $\rho_w(NH_2)$, and was assigned to the frequency at 583 cm^{-1} which displayed the largest $^{14}N/^{15}N$ isotope shift (−9.8 cm^{-1}) (calcd, −9.6 cm^{-1}). This value is comparable to that calculated for F_5TeNF_2 (569 cm^{-1}) and for other dialkylamino derivatives F_5TeNR_2 (538−629 cm^{-1}).[56] The umbrella mode $\delta(TeF_{4e})$ was calculated at 337 cm^{-1} but was not observed. The N−Te−F bends appear in the same region (200−340 cm^{-1}) as the bending modes in TeF_6 (200−330 cm^{-1}) and the NH_2 torsion is assigned to the band at 68 cm^{-1}.

(b) $[F_5TeNH_3][AsF_6]$ and $[^{15}N][F_5TeNH_3][AsF_6]$. The 24 vibrational modes of $F_5TeNH_3^+$ under C_s point symmetry (see Computational Results) belong to the irreducible representations 15A′ + 9A″, which are all Raman and infrared active, and the 15 vibrational modes of AsF_6^- under O_h symmetry (see X-ray Crystal Structures of F_5TeNH_2, $[F_5TeNH_3][AsF_6]$, and $[F_5TeN(H)Xe][AsF_6]$) belong to the irreducible representations $A_{1g} + E_g + T_{2g} + 2T_{1u} + T_{2u}$, where the A_{1g}, E_g, and T_{2g} modes are Raman active and the T_{1u} modes are infrared active.

In the crystal structure of $[F_5TeNH_3][AsF_6]$, two cations and four anions occupy C_s sites, two cations occupy C_1 sites, and two anions occupy C_i sites. The full factor-group analysis

(56) Fraser, G. W.; Peacock, R. D.; Watkins, P. M. *Chem. Commun.* **1967**, 1248.

is provided in Table S7 which predicts that the Raman- and infrared-active vibrational modes of AsF_6^- under both C_s and C_i site symmetries are extensively split as a result of site symmetry lowering and vibrational coupling within the crystallographic unit cell. Correspondingly, all anion modes in the Raman spectrum exhibited splittings. No cation mode splittings are expected under C_s site symmetry in the Raman and infrared spectra of $F_5TeNH_3^+$, whereas the Raman- and infrared-active modes are expected to be split into $A_g + B_g$ and $A_u + B_u$ components, respectively, under C_1 site symmetry. In practice, factor−group splittings were only resolved on two of the cation modes, $\delta_{sym}(NH_3)$ inversion (1397, 1406 cm^{-1}) and $\nu(Te-F_e)$ (683, 689 cm^{-1}) (Table 6).

The calculated NH_3 group frequencies are overestimated at both the DFT and HF levels with the exception of the $\delta_{sym}(NH_3)$ inversion at the DFT level. The decreases in NH_3 group frequencies upon protonation of F_5TeNH_2 are similar to those observed upon protonation of ammonia (NH_3[57] and NH_4^+ [58]) and also occur for all other vibrational frequencies. The Te−N stretch is decoupled from the Te−F stretches and observed at 566 cm^{-1}. The large experimental shift (−15.7 cm^{-1}) is in good agreement with the predicted $^{14}N/^{15}N$ isotope shift (−13.0 cm^{-1}). The Te−F stretches fall in the same range as those of F_5TeNH_2, but the Te−F_a stretch calculated at 736 cm^{-1} is no longer coupled to the Te−F_e stretches. The TeF_5 bends fall in the same range as those of F_5TeNH_2 and TeF_6. The torsion of the NH_3 group has been tentatively assigned to the broad band at 203 cm^{-1}.

(c) $[F_5TeN(H)Xe][AsF_6]$ and $[^{15}N][F_5TeN(H)Xe][AsF_6]$. The $F_5TeN(H)Xe^+$ cation (C_1 symmetry) possesses 21 fundamental vibrational modes belonging to *A* irreducible representations which are both Raman and infrared active. The AsF_6^- anion is distorted from O_h symmetry in the crystal structure as a result of the fluorine bridge interaction with the cation (see X-ray Crystal Structures of $[F_5TeN(H)Xe][AsF_6]$), and therefore its vibrational spectrum may also be assigned under C_1 symmetry. In the latter instance, 15 vibrational modes are expected which belong to *A* irreducible representations. A factor−group analysis correlating the free cation or anion symmetry (C_1) to the crystal site symmetry (C_1) and to the unit cell symmetry (C_i) predicts that no splitting should be observed for either the cation or the anion (Table S8).

The calculated frequencies referred to are those of the isolated cation because the Xe···F_b bond length in the calculated ion pair was far too short (see Computational Results) making the associated vibrational frequencies unreliable. Otherwise, there is good agreement between the calculated and experimental structures and frequencies (Table 7). The highest-frequency band is assigned to ν(NH) (3146 cm^{-1}) and is similar to the NH stretches in secondary amines,[59] F_2NH (3193 cm^{-1}),[60] Cl_2NH (3279 cm^{-1}),[61] F_5TeNH_2 (3297 cm^{-1}, symmetric; 3385 cm^{-1}, antisymmetric), $F_5TeNH_3^+$ (3018 cm^{-1}, symmetric; 3110 cm^{-1}, antisymmetric), and $F_5TeN(H)Si(CH_3)_3$ (3361 cm^{-1}).[14] The H−N−Te bend was observed at 1271 cm^{-1}, while the NH inversion frequency was calculated at 757 cm^{-1} but was not observed. The calculated asymmetric and symmetric combinations for the Te−F_e stretches are similar to those calculated for $F_5TeNH_3^+$ and occurred in the 650−750 cm^{-1} region. The antisymmetric and symmetric combinations of the ν(Xe−N) and ν(Te−N) stretches were observed at 654 and 444 cm^{-1}, respectively, as the two most intense bands in the spectrum, bracketing the experimental Te−N stretching frequency of $F_5TeNH_3^+$ (566 cm^{-1}). Moreover, the observed (−9.5, −10.9 cm^{-1}) and calculated (−15.8, −11.5 cm^{-1}) isotopic shifts are also in good agreement. These fundamental frequencies are comparable, but lower than those in $XeOTeF_5^+$ (exptl, 714 and 487 cm^{-1}; calcd, 680 and 485 cm^{-1}), where the observed modes were also intense. The F−Te−F and F−Te−N bends, which are often coupled, occurred between 170 and 370 cm^{-1}. The bend, δ(Xe−N−Te), is assigned to the band at 113 cm^{-1}, which is slightly lower than that observed for δ(Xe−O−Te) (127 cm^{-1}). The torsion about the Te−N bond was tentatively assigned to the broad band at 90 cm^{-1} and is low as a result of the large masses of the F_5Te group and Xe atom.

Conclusions

The $F_5TeN(H)Xe^+$ cation has been obtained by reaction of XeF_2 with $F_5TeNH_3^+$ in HF and BrF_5 solvents, providing the first example of a synthesis that makes use of an ammonium derivative as the precursor to a compound containing a Xe−N bond, and by reaction of the XeF^+ cation with F_5TeNH_2 in anhydrous HF. The solution and solid-state characterization of the $F_5TeN(H)Xe^+$ cation as the AsF_6^- salt provides the first example of xenon bonded to sp^3-hybridized nitrogen that has been structurally characterized by X-ray crystallography. The $F_5TeN(H)Xe^+$ cation is markedly less stable than the isoelectronic F_5TeOXe^+ [42] cation and is among the least stable Xe−N bonded species reported to date. Its relative instability is attributed to the lower electronegativity of the $F_5TeN(H)$ ligand, which is reflected in the high shielding of the ^{129}Xe NMR resonance of $F_5TeN(H)Xe^+$ relative to that in F_5TeOXe^+, and is consistent with the Xe−N bond in this cation being one of the most covalent Xe−N bonds known. The proposed decomposition route is consistent with the high covalent character of the Xe(II)−N bond and involves Xe gas elimination with the formation of a transient nitrenium ion, F_5TeNH^+. Nucleophilic attack at the nitrogen of the nitrenium ion by a fluoride ion donor leads to Xe gas formation and the formation of the novel fluoramine, F_5TeNF_2.

Experimental Section

Apparatus and Materials. All manipulations were performed under strictly anhydrous conditions as previously described.[43]

(57) Reding, F. P.; Hornig, D. F. *J. Chem. Phys.* **1954**, *22*, 1926.
(58) Shurvell, H. F.; Brown, R. J. C.; Fredericks, P. M.; Rintoul, L. *J. Raman Spectrosc.* **2001**, *32*, 219.
(59) Bellamy, L. J. *Infrared Spectra of Complex Molecules*; John Wiley & Sons: New York, 1954; p 213.
(60) Comeford, J. J.; Mann, D. E.; Schoen, L. J.; Lide, D. R., Jr. *J. Chem. Phys.* **1963**, *38*, 461.
(61) Moore, G. E.; Badger, R. M. *J. Am. Chem. Soc.* **1952**, *74*, 6076.

Literature methods were used to prepare AsF_5,[62] XeF_2,[63] and $[XeF][AsF_6]$[16] and to purify HF[10] (Harshaw Chemical Co.), BrF_5[10] (Ozark-Mahoning Co.), and SO_2[64] (Canadian Liquid Air, Ltd.). Natural abundance and ^{15}N-enriched (99.5%) F_5TeNH_2[14] and $F_5TeNHSi(CH_3)_3$[14] were prepared from $^{15}NH_3$ using scaled-down versions of the procedures reported for the nonenriched compounds. Nitrogen-15-enriched NH_3 was prepared according to the method of Schenk[65] by treating $[^{15}NH_4][Cl]$ (99.5 at. % ^{15}N; Isotech, Inc.) with concentrated aqueous KOH, and it was dried by vacuum distillation at −78 °C into a −196 °C trap.

Natural Abundance and ^{15}N-Enriched $[F_5TeNH_3][AsF_6]$. The title compounds were prepared by protonation of natural abundance and 99.5% ^{15}N-enriched F_5TeNH_2 in HF acidified with excess AsF_5. In a typical synthesis, 1.1873 g (4.976 mmol) of F_5TeNH_2 was loaded into a $^1/_2$ in. o.d. FEP reaction vessel equipped with a 316 stainless steel valve (Whitey ORM2) inside a drybox. Anhydrous HF (4 mL) was condensed onto F_5TeNH_2 at −196 °C and warmed to −78 °C to give a colorless solution. Arsenic pentafluoride (6.1 mmol) was condensed onto the frozen solution at −196 °C and warmed to −55 °C to give a colorless solution. Excess AsF_5 and HF were removed under vacuum at −78 to −40 °C, yielding $[F_5TeNH_3][AsF_6]$ as a white powder (2.0442 g, 95.8% yield) with no detectable vapor pressure at room temperature. The salt is stable indefinitely under anhydrous conditions at room temperature and hydrolyzes rapidly in moist air.

Natural Abundance and ^{15}N-Enriched $[F_5TeN(H)Xe][AsF_6]$ and F_5TeNF_2 for NMR Spectroscopy. Identical conditions were used to prepare NMR samples of natural abundance and ^{15}N-enriched $[F_5TeN(H)Xe][AsF_6]$ for characterization by multi-NMR spectroscopy. In a typical synthesis, stoichiometric amounts of F_5TeNH_2 (0.02567 g, 0.1076 mmol) and $[XeF][AsF_6]$ (0.03630 g, 0.1070 mmol) were loaded into a 4 mm o.d. FEP tube at −196 °C, followed by vacuum distillation of HF (ca. 0.2 mL) into the tube. In a typical synthesis, a sample was prepared in a 9 mm o.d. FEP tube in a similar manner using 0.1428 g (0.5984 mmol) of F_5TeNH_2 and 0.2010 g (0.5926 mmol) of $[XeF][AsF_6]$ combined with ca. 1.5 mL of HF solvent. The tubes were sealed under vacuum at −196 °C, followed by warming to −35 °C for ca. 50 min, which resulted in pale yellow supernatants and white and yellow crystalline precipitates. Spectra were obtained at temperatures between −45 and −32 °C. Samples were also prepared by combining similar molar quantities of $[F_5TeNH_3][AsF_6]$ and XeF_2 using the same solvent and temperature conditions.

Samples for NMR spectroscopy in BrF_5 solvent were prepared by combining, at −196 °C, molar amounts of $[F_5TeNH_3][AsF_6]$ and XeF_2 similar to those used for the syntheses in HF solvent (vide supra). Approximately 0.3 and 1.5 mL of BrF_5 solvent was then vacuum distilled into the 4 mm and 9 mm o.d. FEP tubes, respectively, at −196 °C. After they were sealed under dynamic vacuum at −196 °C, the tubes were warmed to −40 °C for 10 min resulting in pale yellow solutions. NMR spectra were obtained at temperatures between −58 and −44 °C. Complete decomposition of $F_5TeN(H)Xe^+$ in BrF_5 solvent occurred after several hours at −44 °C, as indicated by the intense purple color of the solutions and the absence of the ^{19}F NMR resonances.

Natural Abundance and ^{15}N-Enriched $[F_5TeN(H)Xe][AsF_6]$ for Raman Spectroscopy. Identical procedures were used for the isolation of natural abundance and 99.5% ^{15}N-enriched $[F_5TeN(H)Xe][AsF_6]$. In a typical synthesis, XeF_2 (0.0660 g, 0.390 mmol) and $[F_5TeNH_3][AsF_6]$ (0.1716 g, 0.3995 mmol) were added to a 4 mm o.d. FEP tube fused at right angles to a $^1/_2$ in. o.d. FEP reaction tube which was flare-fitted to a Kel-F valve. The 4 mm o.d. tube was maintained at −196 °C to prevent reaction of the solids. Anhydrous HF (ca. 0.5 mL) was vacuum distilled onto the reagents resulting in a colorless solution at −40 °C. The solution was warmed to −36 °C resulting in a pale yellow solution after 5 min. The yellow color is attributed to the formation of $F_5TeN(H)Xe^+$. Alternatively, similar molar amounts of $[XeF][AsF_6]$ and F_5TeNH_2 were combined in HF solvent and resulted in similar solution compositions. The use of either approach resulted in orange crystals of $[F_5TeN(H)Xe][AsF_6]$ being deposited from solution after ca. 40 min, leaving a pale yellow supernatant. Cooling to −40 °C resulted in the deposition of more crystalline material of the same morphology and color after ca. 10 min. Samples were not cooled below −40 °C because colorless $[F_5TeNH_3][AsF_6]$ began to crystallize. The $^1/_2$ in. o.d. FEP portion of the T-shaped reactor was cooled to −78 °C, and the yellow supernatant was decanted into it. Care was taken to prevent warming of the orange crystals above −40 °C, where slow decomposition began to occur. Both arms of the FEP apparatus were then cooled to −196 °C, and the tube containing the supernatant was separated from the apparatus by heat sealing it off under dynamic vacuum. The orange crystalline precipitate, $[F_5TeN(H)Xe][AsF_6]$, was pumped under high vacuum at −50 °C for 20 h to ensure complete removal of HF solvent.

Crystal Growth. (a) $[F_5TeNH_3][AsF_6]$ and $[F_5TeN(H)Xe][AsF_6]$. In the drybox, F_5TeNH_2 (0.1837 g, 0.770 mmol) and $[XeF][AsF_6]$ (0.2657 g, 0.783 mmol) were loaded into one arm of a $^1/_2$ in. o.d. FEP T-shaped reactor at −160 °C and fitted with a Kel-F valve. The reaction vessel was maintained at −78 °C or below to prevent reaction of the solids. Anhydrous HF (ca. 1 mL) was condensed onto the solids at −196 °C and maintained at −48 °C to effect dissolution. A pale yellow solution initially formed at −48 °C from which colorless, microcrystalline $[F_5TeNH_3][AsF_6]$ precipitated after ca. 1 min. The $[F_5TeNH_3][AsF_6]$ dissolved upon agitation at −48 °C. The reactor was attached to a vacuum line and pressurized with ca. 1 atm of dry nitrogen. The arm containing the solution mixture was inclined at ca. 20° inside the glass dewar of a crystal growing apparatus, which has been described in ref 66, and maintained at −40 °C. After 10 min, the yellow color of the solution intensified and colorless crystals of $[F_5TeNH_3][AsF_6]$ began to grow on the walls of the FEP vessel. The solution was then slowly cooled over a period of 1 h to −53 °C. Lustrous, orange needle-shaped crystals, which proved to be $[F_5TeN(H)Xe][AsF_6]$, formed throughout the solution, resulting in a near colorless supernatant. The solution was maintained at −55 °C for a further 2 h to allow for more complete deposition of crystalline $[F_5TeN(H)Xe][AsF_6]$. The crystals were isolated by decanting the solvent and mounted at low temperature as previously described.[66] Care was taken to prevent warming of $[F_5TeN(H)Xe][AsF_6]$ above −40 °C, where slow decomposition began to occur. A crystal of $[F_5TeNH_3][AsF_6]$ and two $[F_5TeN(H)Xe][AsF_6]$ crystals having the dimensions 0.4 × 0.15 × 0.1 and 0.8 × 0.16 × 0.15/0.22 × 0.08 × 0.07 mm^3, respectively, were selected for X-ray structure determinations.

(b) β-F_5TeNH_2. Crystals of β-F_5TeNH_2 were obtained by static vacuum sublimation into 0.5 mm o.d. Pyrex glass capillaries over

(62) Emara, A. A. A.; Lehmann, J. F.; Schrobilgen, G. J. *J. Fluorine Chem.* **2005**, *126*, 1373.
(63) Mercier, H. P. A.; Sanders, J. C. P.; Schrobilgen, G. J.; Tsai, S. S. *Inorg. Chem.* **1993**, *32*, 386.
(64) Collins, M. J.; Schrobilgen, G. J. *Inorg. Chem.* **1985**, *24*, 2608.
(65) Schenk, P. W. In *Handbook of Preparative Inorganic Chemistry*, 2nd ed.; Brauer, G., Ed.; Academic Press: New York, 1963; Vol. 1, pp 461−463.
(66) Gerken, M.; Dixon, D. A.; Schrobilgen, G. J. *Inorg. Chem.* **2000**, *39*, 4244.

a period of several days. The capillaries were heat-sealed under ca. 1 atm of dry N_2 while the crystals were kept at room temperature. At room temperature, crystals of β-F_5TeNH_2 diffracted well, but when cooled to −14 (± 2) °C, a phase transition occurred which resulted in powdering. The crystal used for the data acquisition at −5 °C had dimensions of 0.35 × 0.26 × 0.12 mm^3. Examination of the crystalline F_5TeNH_2 in a drybox at room temperature revealed that the material exhibited plastic behavior, consistent with a disordered structure.

(c) α-F_5TeNH_2. Crystals of α-F_5TeNH_2 were grown between −50 and −70 °C over a period of several hours from liquid SO_2 in a T-shaped glass vessel and were isolated by decantation into the side tube of the vessel at −78 °C and heat sealed. Any residual SO_2 remaining in the crystalline sample was pumped off under dynamic vacuum at −75 °C followed by pressurization of the reaction vessel to ca. 1 atm with dry nitrogen and maintainence at −78 °C until the crystals could be mounted at low temperature as previously described.[66] The crystals were large and several were cut into smaller fragments. The crystal fragment used for the data acquisition had dimensions of 0.15 × 0.08 × 0.02 mm^3.

X-ray Crystallography. (a) Collection and Reduction of X-ray Data. The crystals were centered on a P4 Siemens diffractometer, equipped with a Siemens SMART 1K charge-coupled device (CCD) area detector using the program SMART[67] and a rotating anode using graphite-monochromated Mo Kα radiation ($\lambda = 0.71073$ Å). The diffraction data collection consisted of a full ψ rotation at $\chi = 0°$ using (1200 + 50) 0.3° frames, followed by a series of short (100 frames) ω scans at various ψ and χ settings to fill the gaps. The crystal-to-detector distance was 5.000 cm, and the data collection was carried out in a 512 × 512 pixel mode using 2 × 2 pixel binning. Processing was carried out by using the program SAINT,[67] which applied Lorentz and polarization corrections to three-dimensionally integrated diffraction spots. The program SADABS[68] was used for the scaling of diffraction data, the application of a decay correction, and an empirical absorption correction based on redundant reflections. The data set used in the solution of $[F_5TeN(H)Xe][AsF_6]$ was obtained by combination of two data sets obtained from two single crystals using the program XPREP.[69] A total of 2202 unique reflections remained after combination of their unique reflections.

(b) Solution and Refinement of the Structures. The XPREP program was used to confirm the unit cell dimensions and the crystal lattice. The final refinement for most of the structures was obtained by introducing anisotropic parameters for all the atoms (except the hydrogen atoms), an extinction parameter, and the recommended weight factor. The maximum electron densities in the final difference Fourier maps were located around the heavy atoms. All calculations were performed using the SHELXL package for structure determination, refinement, and molecular graphics.[69]

A solution was obtained for $[F_5TeNH_3][AsF_6]$, α-F_5TeNH_2 and β-F_5TeNH_2 by direct methods and using a Patterson function for $[F_5TeN(H)Xe][AsF_6]$ which located both the Te and As atoms. Successive difference Fourier syntheses revealed the positions of all the fluorine and nitrogen atoms which were assigned on the basis of their bond lengths with tellurium. In the case of β-F_5TeNH_2, the solution involved a 6-fold disorder (site occupancy fixed to 0.20833 for F/N and 0.04167 for N/F). The positions of the hydrogen atoms were calculated (d(N−H) ≈ 0.82 Å; U(H) fixed to $-1.5U$(N)) and were then refined using AFIX ($F_5TeNH_3^+$) and DFIX (α-F_5TeNH_2 and $F_5TeN(H)Xe^+$) restraints.[69]

Nuclear Magnetic Resonance Spectroscopy. All NMR spectra were recorded unlocked (field drift < 0.1 Hz h^{-1}) with the use of Bruker AC-300 (7.0463 T) and AM-500 or Avance DRX-500 (11.7440 T) spectrometers. Spectra were recorded at low temperatures on samples in heat-sealed 9 mm o.d. or 4 mm o.d. FEP NMR tubes, which were placed inside precision 10 mm and 5 mm glass NMR tubes.

Xenon-129, ^{15}N, and ^{125}Te NMR spectra at 11.7440 T were recorded in 9 mm o.d. FEP sample tubes using a 10-mm probe broad-banded over the frequency range of 23−202 MHz tuned to 139.051 (^{129}Xe), 50.698 (^{15}N), or 157.795 (^{125}Te) MHz. Fluorine-19 (470.599 MHz) and proton (500.138 MHz) spectra (11.7440 T) were recorded in 4 mm o.d. FEP tubes using a 5 mm dual ^{1}H/^{19}F probe. Xenon-129 and ^{1}H NMR spectra (7.0463 T) were recorded in 9 mm o.d. FEP tubes using a 10 mm probe broad-banded over the frequency range of 14−121 MHz tuned to 83.468 (^{129}Xe) and 300.144 (^{1}H) MHz. Pulse widths corresponding to bulk magnetization tip angles (μs) of ∼90° were 18.0 (11.7440 T) and 14.0 (7.0463 T) for ^{129}Xe, 1.0 (11.7440 T) for ^{19}F, 10.0 (11.7440 T) for ^{125}Te, 15.0 (11.7440 T) for ^{15}N, and 5.0 (11.7440 T) and 2.0 (7.0463 T) for ^{1}H. Line broadening parameters used in exponential multiplication of the free induction decays were set equal to or less than their respective data point resolutions or the natural line widths of the resonances. All line shape functions were Lorentzian unless specified, where the free induction decays were multiplied by Gaussian functions for resolution enhancement on Fourier transformation. Detailed acquisition parameters are provided in the Supporting Information.

The ^{129}Xe−^{1}H INEPT spectrum of $[^{15}N][F_5TeN(H)Xe][AsF_6]$ in HF solvent was recorded at 83.468 MHz (7.0463 T) using a 10 mm probe broad-banded over the frequency range of 14−121 MHz. The spectrum was acquired over a 15 kHz spectral width in 2 K data points (0.682 s acquisition time and a data point resolution of 1.5 Hz/pt). The INEPT pulse sequence was used with a ^{129}Xe 90° pulse width of 14.0 μs. The ^{1}H 90° pulse width through the decoupler channel was 20.0 μs. The fixed delay in the INEPT pulse sequence ($0.25\{1/[^2J(^{129}Xe-^1H)]\}$) was 0.01086 s with a relaxation delay of 1.0 s. The free induction decays were zero-filled to 8 K data points and processed using Gaussian multiplication for resolution enhancement (line broadening, −2.5 Hz; Gaussian broadening, 0.35 s) before Fourier transformation. Details of the acquisition parameters are provided in the Supporting Information.

The respective nuclei were referenced externally to neat samples of $XeOF_4$ (^{129}Xe), $CFCl_3$ (^{19}F), natural abundance CH_3NO_2 (^{15}N), $Te(CH_3)_2$ (^{125}Te), and $(CH_3)_4Si$ (^{1}H) at 30 °C. Positive chemical shifts were assigned to resonances occurring at higher frequency than those of the reference substances.

Raman Spectroscopy. The Raman spectra were recorded at −160 to −165 °C in 4 mm o.d. reaction vessels in the macrosample chamber of a Jobin-Yvon Mole S-3000 triple spectrograph system equipped with a CCD detector, using the 514.5 nm line of an Ar^+ ion laser at ≤210 mW to avoid sample decomposition. The instrumental details and the method for maintaining the sample at low temperature are reported elsewhere.[70] Slit settings corresponded to a resolution of 0.5 cm^{-1} and a total of 20−30 reads with 10−40 s integration times were summed for each Raman spectrum.

Computational Methods. The calculations were done at the density functional theory (DFT) level with both local (LDFT) and

(67) *SMART* and *SAINT*, release 4.05; Siemens Energy and Automation, Inc.: Madison, WI, 1996.
(68) Sheldrick, G. M. *SADABS* (Siemens Area Detector Absorption Corrections); Personal communication, 1996.
(69) Sheldrick, G. M. *SHELXTL-Plus*, release 5.03; Siemens Analytical X-ray Instruments, Inc.; Madison, WI, 1994.
(70) Casteel, W. J., Jr.; Kolb, P.; LeBlond, N.; Mercier, H. P. A.; Schrobilgen, G. J. *Inorg. Chem.* **1996**, *35*, 929.

gradient-corrected functionals, at the molecular orbital theory Hartree−Fock level, and at the correlated MP2 level. The DFT calculations were done with the program DGauss[71−74] and Gaussian[45] on SGI computers and with the program NWChem[75] on a large HP Linux cluster. For the initial LDFT calculations,[76] the DZVP2 basis set[77] for H, N, O, and F was used and for Te and Xe, a basis set in which the Kr core electrons are treated with a pseudopotential (PP) and the remaining electrons are treated with a polarized valence double-ζ basis set.[78,79] All electron calculations using the DZVP basis set led to Te−F and Te−N bond distances that were too long by about 0.1 Å. Additional DFT calculations with the local correlation-exchange functional were done for F_5TeNH_2 and $F_5TeN(H)Xe^+$ with the Hay−Wadt effective core potentials (ECPs) on Te and Xe and the appropriate ECP basis sets augmented by d functions[44] with the DZVP2 basis set for the other atoms. These calculations led to geometries similar to the all-electron calculations with bond distances that were too long.

The HF calculations were done with the program system Gaussian98.[45] The HF calculations were done with the Hay−Wadt effective core potentials (ECPs) on Te and Xe and basis sets, and for the remaining atoms, the polarized valence double-ζ basis set of Dunning and Hay was used.[46] The natural bond orbital (NBO) analysis[47−51] was done at the DFT level with the polarized valence double-ζ basis set[46] for H, N, O, and F and an all-electron basis set from Huzinaga et al.[80] contracted to valence polarized double-ζ was used for Te and Xe.

In the course of this work, the correlation consistent basis sets originally developed by Dunning[81] were extended to heavier main-group elements by Peterson and co-workers[82,83] in combination with effective core potentials from the Stuttgart group for all of the main group atoms. An additional set of calculations was performed on the more problematic ion-pair structures and the related cation with the aug-cc-pVDZ basis set[84] for the light atoms and the aug-cc-pVDZ-PP basis set for the heavier atoms. The calculations were done at the HF, MP2,[85] local DFT, and gradient-corrected (B3LYP)[86,87] levels for a number of structures with the program system NWChem. The methods were benchmarked for TeF_6 as described in the Supporting Information.

Acknowledgment. This paper is dedicated to our friend and colleague, Professor Karl O. Christe, on the occasion of his 70th birthday. We thank the donors of the Petroleum Research Fund, administered by the American Chemical Society, for support of part of this work under Grant ACS-PRF No. 33594-AC3. The computational portion of this research was performed, in part, using the Molecular Science Computing Facility in the William R. Wiley Environmental Molecular Sciences Laboratory at the Pacific Northwest National Laboratory, Richland, WA under U.S. Department of Energy contract DE-AC06-76RLO 1830. We thank the Natural Sciences and Engineering Research Council (NSERC) of Canada for financial support in the form of a research grant, and NSERC and the Ontario Ministry of Colleges and Universities for the award of graduate scholarships to J.M.W. We also thank Dr. D. W. Hughes, McMaster University NMR Facility, for help with the ^{15}N and ^{129}Xe INEPT experiments.

Supporting Information Available: Discussion of the calculated geometric parameters, the use of TeF_6 as a benchmark. detailed NMR acquisition parameters, bond lengths and bond angles for the AsF_6^- anion in $[F_5TeNH_3][AsF_6]$, $[F_5TeN(H)Xe][AsF_6]$ (Table S1), experimental and calculated bond lengths for $F_5TeN(H)Xe^+$ and $[F_5TeN(H)Xe][AsF_6]$ (Table S2), vibrational frequencies (cm^{-1}) for F_5TeN^{2-} (Table S3), NBO analysis (Table S4) for $F_5TeNH_3^+$, $F_5TeN(H)Xe^+$, F_5TeNH_2, F_5TeNF_2, and F_5TeN^{2-}, Raman spectra of unreacted $[F_5TeNH_3][AsF_6]$ and $[Xe_2F_3][AsF_6]$ in $[F_5TeN(H)Xe][AsF_6]$ (Table S5), correlation diagrams for the vibrational modes of F_5TeNH_2 (Table S6), $[F_5TeNH_3][AsF_6]$ (Table S7), and $[F_5TeN(H)Xe][AsF_6]$ (Table S8), proton NMR spectrum of $[F_5TeNH_3][AsF_6]$ (Figure S1), ^{19}F NMR spectrum of $[F_5TeNH_3][AsF_6]$ (Figure S2), ^{15}N NMR spectrum of $[F_5Te^{15}NH_3][AsF_6]$ (Figure S3), ^{125}Te NMR spectrum of $[F_5TeNH_3][AsF_6]$ (Figure S4), Raman spectra of F_5TeNH_2 and $F_5Te^{15}NH_2$ (Figure S5), Raman spectrum of $[F_5TeNH_3][AsF_6]$ and $[F_5Te^{15}NH_3][AsF_6]$ (Figure S6), and an X-ray crystallographic file in CIF format for the structure determinations of $[F_5TeNH_3][AsF_6]$, $[F_5TeN(H)Xe][AsF_6]$, and α- and β-F_5TeNH_2. This material is available free of charge via the Internet at http://pubs.acs.org.

IC051451T

(71) Andzelm, J.; Wimmer, E.; Salahub, D. R. In *The Challenge of d and f Electrons: Theory and Computation*; Salahub, D. R., Zerner, M. C., Eds.; ACS Symposium Series 394; American Chemical Society: Washington, DC, 1989; p 228.
(72) Andzelm, J. In *Density Functional Theory in Chemistry*; Labanowski, J., Andzelm, J., Eds.; Springer-Verlag: New York, 1991; p 155.
(73) Andzelm, J. W.; Wimmer, E. *J. Chem. Phys.* **1992**, *96*, 1280.
(74) Komornicki, A.; Fitzgerald, G. *J. Phys. Chem*. **1993**, *98*, 1398.
(75) Aprà, E.; Bylaska, E. J.; de Jong, W.; Hackler, M.; Hirata, S.; Pollack, L.; Smith, D. M. A.; Straatsma, T. P.; Windus, T. L.; Harrison, R.; Nieplocha, J.; Tipparaju, V.; Kumar, M.; Brown, E.; Cisneros, G.; Dupuis, M.; Fann, G.; Früchtl, H.; Garza, J.; Hirao, K.; Kendall, R.; Nichols, J.; Tsemekhman, K.; Valiev, M.; Wolinski, K.; Anchell, J.; Bernholdt, D.; Borowski, P.; Clark, T.; Clerc, D.; Dachsel, H.; Deegan, M.; Dyall, K.; Elwood, D.; Glendening, E.; Gutowski, M.; Hess, A.; Jaffe, J.; Johnson, B.; Ju, J.; Kobayashi, R.; Kutteh, R.; Lin, Z.; Littlefield, R.; Long, X.; Meng, B.; Nakajima, T.; Niu, S.; Rosing, M.; Sandrone, G.; Stave, M.; Taylor, H.; Thomas, G.; van Lenthe, J.; Wong, A.; Zhang, Z. *NWChem. PNNL*, 2003.
(76) Vosko, S. J.; Wilk, L.; Nusair, W. *Can. J. Phys*. **1980**, *58*, 1200.
(77) Godbout, N.; Salahub, D. R.; Andzelm, J.; Wimmer, E. *Can. J. Chem.* **1992**, *70*, 560.
(78) Chen, H.; Kraskowski, M.; Fitzgerald, G. *J. Chem. Phys*. **1993**, *98*, 8710.
(79) Troullier, N.; Martins, J. L. *Phys. Rev. B* **1991**, *43*, 1993.
(80) *Gaussian Basis Sets for Molecular Calculations*; Huzinaga, S., Andzelm, J., Klobukowski, M., Radzio-Andzelm, E., Sakai, Y., Tatewaki, H., Eds.; Physical Sciences Data 16; Elsevier: Amsterdam, 1984.
(81) Dunning, T. H., Jr. *J. Chem. Phys.* **1989**, *90*, 1007.
(82) Peterson, K. A. *J. Chem. Phys.* **2003**, *119*, 11099.
(83) Peterson, K. A.; Figgen, D.; Goll, E.; Stoll, H.; Dolg, M. *J. Chem. Phys.* **2003**, *119*, 11113.
(84) Kendall, R. A.; Dunning, T. H., Jr.; Harrison, R. J. *J. Chem. Phys.* **1992**, *96*, 6796.
(85) Frisch, M. J.; Head-Gordon, M.; Pople, J. A. *Chem. Phys. Lett.* **1990**, *166*, 275.
(86) Becke, A. D. *Phys. Rev. A* **1988**, *38*, 3098.
(87) Lee, C.; Yang, W.; Parr, R. G. *Phys. Rev. B* **1988**, *37*, 785.